J. Fluid Mech. (1999), *vol.* 381, *pp.* 89–119. Printed in the United Kingdom

The transient period for boundary layer disturbances

By D. G. LASSEIGNE[1], R. D. JOSLIN[2], T. L. JACKSON[3]† AND W. O. CRIMINALE[4]

[1]Department of Mathematics and Statistics, Old Dominion University, Norfolk, VA 23529, USA

[2]Fluid Mechanics and Acoustics Division, NASA Langley Research Center, Hampton, VA 23681-0001, USA

[3]Institute for Computer Applications in Science and Engineering, NASA Langley Research Center, Hampton, VA 23681-0001, USA

[4]Department of Applied Mathematics, University of Washington, Seattle, WA 98195, USA

(Received 24 January 1998 and in revised form 20 August 1998)

The onset of transition in a boundary layer is dependent on the initialization and interaction of disturbances in a laminar flow. Here, theory and full Navier–Stokes simulations focus on the transient period just after disturbances enter the boundary layer. The temporal evolution of disturbances within a boundary layer is investigated by examining a series of initial value problems. In each instance, the complete spectra (i.e. the discrete and the continuum) are included so that the solutions can be completely arbitrary. Both numerical and analytical solutions of the linearized Navier–Stokes equations subject to the arbitrary initial conditions are presented. The temporal evolution of disturbances during the transient period are compared with the spatial evolution of the same disturbances and a strong correlation between the two approaches is demonstrated indicating that the theory may be used for the transient period of disturbance evolution. The theory and simulations demonstrate that strong amplification of the disturbances can occur as a result of the inclusion of the continuum in the prediction of disturbance evolution. The results further show that any approach proposed for use in bypass boundary layer transition must include the transient growth that results from the continuum. Finally, although a connection between temporal and spatial evolution in the transient period has been demonstrated, a theoretical basis as an explanation for this connection remains the focus of additional study.

1. Introduction

The laminar boundary layer on a flat plate continues to be one of the most essential prototypical shear flows in fluid mechanics. This flow is important not only because it is a concept that has vast utility in many diverse physical situations, but also because it is a flow that can be (and has been) probed extensively by use of all available means from theory and experiment to numerical simulation. Still, even after nearly a full century that has been spent in such effort, a complete and thorough understanding of the behaviour of the flow in the presence of perturbations has not been obtained. Many important questions remain to be answered before progress towards such goals

† Current address: Center for Simulation of Advanced Rockets, 3244 DCL, College of Engineering, University of Illinois, 1304 West Springfield Ave., Urbana, IL 61801, USA.

as positive control disturbances in the flow or a means of retarding the transition from a laminar to a turbulent state can be fully utilized in a practical configuration.

Traditionally, investigations of disturbances in the boundary layer have been characterized using classical linear stability analysis. This concept is well founded and is, in principle, correctly recognized as an initial-value problem. However, few real calculations have actually been made in this pursuit, that is, calculations directed at examining the details of specific initial-value problems. Instead, it was considered sufficient to demonstrate that the flow was actually unstable and to determine the physical explanation of the cause of any instability that might result. It was understood that any perturbation that was introduced and regardless of the nature of the origin, would meet the same fate. Once this process had begun, the flow must break down and then ultimately would end in transition to turbulence. It is now known that such conclusions are not necessarily correct and can even be misleading. It is for this reason that a full knowledge of the dynamics of perturbations must be ascertained so that a rational evaluation can be made. In short, it is a moot point that a disturbance will eventually grow to large amplitudes asymptotically in an exponential manner for large time if, during the early transient period, the perturbation behaves quite differently. That such a different behaviour is possible has long been recognized and is directly due to the fact that the bases for this problem are not those of conventional wisdom. Even though linear, the problem presents difficulties for both the analytical and the numerical treatments. Specifically, the differential equations are not self-adjoint (although not presented in terms of the fluid mechanics, the mathematical topic is discussed by one of original workers in this field, namely Sommerfeld 1949) and they are of the stiff variety, making numerical solutions difficult to obtain. Moreover no solution can be expressed by a simple representation – except formally – that makes it amenable for use for arbitrary initial-value calculations.

The details of any particular initial-value specification require far more information than can be derived from the simple fact that the flow is unstable. Indeed, as already suggested, the transient as well as the asymptotic state contains significant information. The essential origins and recognition that the early time period should be noted are due to Kelvin (1887) and Orr (1907*a*,*b*). More recently there has been a flurry of activity in this area since it may be possible that explanations for events that are known to take place during breakdown in the boundary layer may be forthcoming by making a detailed examination of the early period. Results thus far are both suggestive and promising but not necessarily uniformly accepted as the cause of breakdown in the boundary layer. It is the purpose of this study to delve more deeply into many of the details (and use the argument as far as may be rationally possible) as well as put the problem on a firmer mathematical and practical foundation so that other possible cases can be readily analysed. The method is a combined analytical–numerical technique that allows for completely arbitrary initial values. And, although not treated here, the technique has the ability to address the very important question of receptivity of the boundary layer. It is also suggested that the physics is best exploited in terms of the vorticity, a quantity that is more natural than the velocity to problems of this variety.

Many of the extensive contributions that have been made for early-period dynamics are for fully bounded shear flows. By contrast, full attention to the special needs of the boundary layer is lacking. Butler & Farrell (1992) were primarily concerned with optimal perturbation conditions in channel flows. However, using their results found for these cases, they assumed that the boundary layer problem could be similarly resolved by extension. More specifically, since the boundary layer is not bounded

from above as it is in channel flow, there must be a continuous as well as a discrete spectrum of eigenvalues when using normal mode solutions for the linear partial differential equations to represent disturbance evolution in the flow. In recognizing this fact, Butler & Farrell elected to approximate the continuous part of the spectrum by a finite set of available modes and coupled this representation with a modification to the boundary condition that requires disturbances to vanish in the far field. These steps were logical because, when optimal conditions for channel flow were found to be confined to the shear region very close to the walls, it was thought that a similar argument could be made for the boundary layer. It will be shown here that these assumptions will lead to the loss of important critical behaviour in the dynamics.

One early attempt to solve an initial-value problem for the laminar boundary layer in the conventional sense was that due to Criminale & Kovasznay (1962). But, in spite of the fact that it was correctly posed, this effort required significant simplifying assumptions in order to extract any results whatsoever. The framework was in terms of but a few normal modes and the computing was limited. As a result, it was impossible to examine the early period and no mention of the continuous spectrum was made at all. More recently, Breuer & Haritonidis (1990) made a far more advanced investigation of this flow and it was done in a way that overcame all of the difficulties experienced by Criminale & Kovasznay. The sole weakness here was that the perturbation calculations were made for an inviscid fluid. A sequel paper by Breuer & Kuraishi (1994) rectified this omission. Breuer and co-workers elected to use a numerical scheme that combined a time integration of the linear partial differential equations together with Chebyshev polynomials for the vertical spatial variation rather than invoke the travelling wave modal form that is more common and was used by Butler & Farrell. This scheme avoids the necessity of having to expand in terms of the modes but removes the possibility of any free-stream interaction because Chebyshev polynomials decay quite rapidly in the far field. It will be seen that this constraint is too severe and will lead to the loss of important physics. Instead, as definitively pointed out by Grosch & Salwen (1978) and Salwen & Grosch (1981), perturbations should be considered merely as bounded rather than vanishing far above the plate if one wishes to capture the effects of the continuous spectrum related to the early period temporal behaviour.

Basically the issue for the transient period of the dynamics is the fact that there can be algebraic growth in the amplitude of the perturbations even if there is ultimate decay as time increases further. This has been shown in several ways. First, by using Laplace transforms for the initial-value problem (Gustavsson 1979; Hultgren & Gustavsson 1980), a branch cut as well as poles in the complex plane must be evaluated when doing the inversions. This immediately denotes that the boundary layer has the additional continuous spectrum and one genesis of algebraic behaviour. Second, the eigenvalue problem that must be solved when using travelling wave modal solutions is not one of the standard Sturm–Liouville form. The principal governing equations are not self-adjoint and hence a system where eigenfunctions are not mutually orthogonal must be anticipated. Thus, even at subcritical values of the Reynolds number, where all eigenvalues are found to cause damping, an initial algebraic growth must occur (Reddy & Henningson 1993; Trefethen *et al.* 1993, among others). Third, there are two equations that must be considered for the full three-dimensional perturbation problem, namely the Squire equation (normal vorticity) together with that of Orr–Sommerfeld (velocity). This combination forms the basis for possible direct resonance between the two sets of solutions and hence algebraic behaviour would ensue. It appears, however, that although this possibility can occur

for channel flows, the numerical calculations of Benney & Gustavsson (1981) have shown that such interplay does not transpire in the boundary layer. Many authors have demonstrated that the early algebraic growth can reach exceptionally large amplitudes on a time scale shorter than that for a growing exponential mode. There is a further belief that this kind of behaviour, even though stemming from a linear system, is actually tantamount to promoting rapid transition and leads to what is now known as bypass transition – strong amplification that is different from that associated with an exponentially growing Tollmien–Schlichting wave.

Besides the general question of transition of the boundary layer, there is the need to understand how this flow interacts with the free stream or, more simply, the receptivity problem. This phenomenon makes this type of flow (as well as unbounded free shear flows) different from that in channels. Not only is the boundary layer unstable but it is clear that the dynamics can be influenced by disturbances, such as vorticity, in the free stream. Due to the fact that the scales for such free-stream disturbances are not at all commensurate with those corresponding to Tollmien–Schlichting waves, analytical treatment of this problem has been difficult as can be seen by the review of Goldstein & Hultgren (1989) for example. In this work it is suggested that the boundary layer should be considered non-parallel or possess a surface roughness in order to gain insight into receptivity. Otherwise, according to this reasoning, there can be no coupling of the boundary layer with the free stream. It will be suggested that an alternative means for exploration of this coupling is also possible and such additional complexities may not be required to initiate the coupling.

Direct numerical simulations (DNS) of the Navier–Stokes equations for boundary-layer flow have for the most part focused on computing the evolution of the discrete-spectrum modes. Generally speaking these studies are directed at transition but at least one has investigated an initial-value problem (Breuer & Landahl 1990). The activity within the boundary layer is captured with DNS almost as if one had been viewing an experiment but the finite limitations of the computational domain have not fully resolved the receptivity problem. Then, many of the numerical studies have been biased by the propensity to Tollmien–Schlichting waves. As has been noted, this kind of process may not be the major cause of breakdown. More intensive work using the general initial-value approach is still in order. In this way, a basis to compare theory with DNS solutions can be established.

The theoretical problem is formulated in §2 and the formal solution in terms of discrete and continuum eigenfunctions is discussed in §3. The numerical method of solution is outlined in §4, and §5 presents results in terms of a normalized perturbation energy for two- and three-dimensional disturbances, as well as a presentation of optimal initial conditions. An analytic solution is presented in §6, and the importance of the initial normal vorticity to the transient growth is evaluated. Results from the temporal theory are compared with the equivalent transient test case in the spatially evolving problem in §7. For the spatial results, a time and spatially accurate direct numerical simulation code is employed. A brief description of the code is also presented in §7. Finally, conclusions are given in §8.

2. Basic governing equations

For the Blasius flat-plate boundary layer, the fluid is incompressible with the basic flow assumed parallel with $U = U(y), V = W = 0$. Then, the non-dimensional linearized equations of motion can be written, with (u, v, w) the perturbation velocity

components in the (x, y, z)-directions and p the perturbation pressure, as

$$\frac{\partial u}{\partial x} + \frac{\partial v}{\partial y} + \frac{\partial w}{\partial z} = 0, \tag{1}$$

$$\frac{\partial u}{\partial t} + U\frac{\partial u}{\partial x} + \frac{\mathrm{d}U}{\mathrm{d}y}v + \frac{\partial p}{\partial x} = R_{\delta^*}^{-1}\left[\frac{\partial^2 u}{\partial x^2} + \frac{\partial^2 u}{\partial y^2} + \frac{\partial^2 u}{\partial z^2}\right], \tag{2}$$

$$\frac{\partial v}{\partial t} + U\frac{\partial v}{\partial x} + \frac{\partial p}{\partial y} = R_{\delta^*}^{-1}\left[\frac{\partial^2 v}{\partial x^2} + \frac{\partial^2 v}{\partial y^2} + \frac{\partial^2 v}{\partial z^2}\right], \tag{3}$$

and

$$\frac{\partial w}{\partial t} + U\frac{\partial w}{\partial x} + \frac{\partial p}{\partial z} = R_{\delta^*}^{-1}\left[\frac{\partial^2 w}{\partial x^2} + \frac{\partial^2 w}{\partial y^2} + \frac{\partial^2 w}{\partial z^2}\right]. \tag{4}$$

Here, $Re = 1.72078764R_{\delta^*}$ is the Reynolds number based on the displacement thickness $\delta^* = \int_0^\infty 1 - U(y)\,\mathrm{d}y$, U_∞ the free-stream velocity and ν the kinematic viscosity. Time is non-dimensionalized by the advective time scale. Using the Fourier transformations defined with respect to x and z, the pertubation velocities can be transferred to wavenumber space as

$$\check{v}(\alpha, y, \beta, t) = \int_{-\infty}^{\infty}\int_{-\infty}^{\infty} v(x, y, z, t)\mathrm{e}^{\mathrm{i}(\alpha x + \beta z)}\,\mathrm{d}x\,\mathrm{d}z, \tag{5}$$

where α_{δ^*} and β_{δ^*} are taken to be real non-dimensional wavenumbers in the x- and z-directions, respectively. The transformations $\alpha = \delta^*\alpha_{\delta^*}$ and $\beta = \delta^*\beta_{\delta^*}$ relate the wavenumbers based on the displacement thickness to these non-dimensional numbers. Substituting (5) into equations (1) to (4) gives

$$-\mathrm{i}(\alpha_{\delta^*}\check{u} + \beta_{\delta^*}\check{w}) + \frac{\partial \check{v}}{\partial y} = 0, \tag{6}$$

$$\frac{\partial \check{u}}{\partial t} - \mathrm{i}\alpha_{\delta^*}U\check{u} + U'\check{v} - \mathrm{i}\alpha_{\delta^*}\check{p} = R_{\delta^*}^{-1}\left[\frac{\partial^2 \check{u}}{\partial y^2} - \tilde{\gamma}_{\delta^*}^2\check{u}\right], \tag{7}$$

$$\frac{\partial \check{v}}{\partial t} - \mathrm{i}\alpha_{\delta^*}U\check{v} + \frac{\partial \check{p}}{\partial y} = R_{\delta^*}^{-1}\left[\frac{\partial^2 \check{v}}{\partial y^2} - \tilde{\gamma}_{\delta^*}^2\check{v}\right], \tag{8}$$

and

$$\frac{\partial \check{w}}{\partial t} - \mathrm{i}\alpha_{\delta^*}U\check{w} - \mathrm{i}\beta_{\delta^*}\check{p} = R_{\delta^*}^{-1}\left[\frac{\partial^2 \check{w}}{\partial y^2} - \tilde{\gamma}_{\delta^*}^2\check{w}\right], \tag{9}$$

with $U' = \mathrm{d}U/\mathrm{d}y$ and $\tilde{\gamma}_{\delta^*}^2 = \alpha_{\delta^*}^2 + \beta_{\delta^*}^2$. Also, $\tilde{\gamma} = \delta^*\tilde{\gamma}_{\delta^*}$.

The Squire transformation is written as

$$\alpha_{\delta^*}\check{u} + \beta_{\delta^*}\check{w} = \tilde{\gamma}_{\delta^*}\tilde{u}, \tag{10}$$

$$-\beta_{\delta^*}\check{u} + \alpha_{\delta^*}\check{w} = \tilde{\gamma}_{\delta^*}\tilde{w}, \tag{11}$$

and combined with operations on (6) to (9) enables one to obtain the pair of equations

$$\left[\frac{\partial}{\partial t} - \mathrm{i}\alpha_{\delta^*}U\right]\left(\frac{\partial^2 \check{v}}{\partial y^2} - \tilde{\gamma}_{\delta^*}^2\check{v}\right) + \mathrm{i}\alpha_{\delta^*}U''\check{v} = R_{\delta^*}^{-1}\left[\frac{\partial^4 \check{v}}{\partial y^4} - 2\tilde{\gamma}_{\delta^*}^2\frac{\partial^2 \check{v}}{\partial y^2} + \tilde{\gamma}_{\delta^*}^4\check{v}\right] \tag{12}$$

and

$$\left[\frac{\partial}{\partial t} - \mathrm{i}\alpha_{\delta^*}U\right]\tilde{w} = \sin\phi U'\check{v} + R_{\delta^*}^{-1}\left[\frac{\partial^2 \tilde{w}}{\partial y^2} - \tilde{\gamma}_{\delta^*}^2\tilde{w}\right], \tag{13}$$

where $U'' = \mathrm{d}^2U/\mathrm{d}y^2$, $\sin\phi = \beta_{\delta^*}/\tilde{\gamma}_{\delta^*}$ and $\tilde{w}$ is proportional to the normal vorticity component ($\check{\omega}_y = \mathrm{i}\tilde{\gamma}_{\delta^*}\tilde{w}$). The first term on the right-hand side of (13) has been denoted as vortex tilting that acts as forcing for the normal vorticity. This term is a product of the mean vorticity in the spanwise direction ($\Omega_z = -U'$) and the perturbation strain rate ($\partial v/\partial z$) and, for a three-dimensional disturbance, gives rise to the increase of the normal vorticity. It is clear that the solutions for (12) and (13) combined with continuity and the Squire transformation are equivalent to solving (6) to (9), including $\check{p}$. In either case, solutions of the equations are subject to imposed initial conditions and the following boundary conditions at the plate:

$$\check{v}(0,t) = \frac{\partial\check{v}}{\partial y}(0,t) = \tilde{w}(0,t) = 0. \tag{14}$$

Furthermore, all disturbances are to be considered bounded in the free stream. For the mean velocity, the Blasius boundary layer solution, with $U(y) = f'(y)$, is assumed and is given by

$$f''' + \tfrac{1}{2}ff'' = 0$$

subject to the conditions

$$f(0) = f'(0) = 0; \qquad f'(\infty) = 1.$$

To evaluate the other velocity components, the quantities $\check{v}$ and $\tilde{w}$ are first computed from (12) and (13). Then the Squire transformation, (10) and (11), when combined with (6) can be inverted to give

$$\check{u} = -\frac{\mathrm{i}\cos\phi}{\tilde{\gamma}_{\delta^*}}\frac{\partial\check{v}}{\partial y} - \sin\phi\tilde{w}, \tag{15}$$

and

$$\check{w} = -\frac{\mathrm{i}\sin\phi}{\tilde{\gamma}_{\delta^*}}\frac{\partial\check{v}}{\partial y} + \cos\phi\tilde{w}. \tag{16}$$

By knowing the velocity, the vorticity perturbations can be determined in a straightforward manner by appealing to the definitions, namely

$$\check{\omega}_x = \frac{\partial\check{w}}{\partial y} + \mathrm{i}\beta_{\delta^*}\check{v}, \tag{17}$$

$$\check{\omega}_y = -\mathrm{i}\beta_{\delta^*}\check{u} + \mathrm{i}\alpha_{\delta^*}\check{w} \equiv \mathrm{i}\tilde{\gamma}_{\delta^*}\tilde{w}, \tag{18}$$

and

$$\check{\omega}_z = -\mathrm{i}\alpha_{\delta^*}\check{v} - \frac{\partial\check{u}}{\partial y} \tag{19}$$

in Fourier space.

Finally, we remark here that, if one seeks solutions for (12) and (13) of the form $\mathrm{e}^{-\mathrm{i}\omega t}f(y)$, then these equations become the more familiar Orr–Sommerfeld and Squire equations. Solutions of these equations are the classical normal modes or travelling wave solutions and usually the transient dynamics and effects of various initial conditions are ignored. However, at subcritical Reynolds numbers, where all normal modes are damped, the transient behaviour may be extremely important as has been shown for viscous channel flows (see Gustavsson 1991; Butler & Farrell 1992; Reddy & Henningson 1993; Criminale *et al.* 1997). Indications of similar importance for the boundary layer have been given by Gustavsson (1979), Hultgren & Gustavsson (1980) and Butler & Farrell (1992).

3. Formal representation of the solution

The solution to (12) and (13) contains both a discrete set of eigenvalues and a continuum and, once an initial condition is prescribed, the solution can be written as a linear combination of the two sets (see Salwen & Grosch 1981). We summarize here only some of the points relevant to the present work.

Salwen & Grosch (1981) provided a completeness argument that showed any solution to (12), together with an initial condition, can be written as

$$\check{v} = \sum_{j=1}^{N} A_j \mathrm{e}^{\mathrm{i}\omega_j t}\phi_j(y) + V_c(y,t), \tag{20}$$

where N is the number of discrete modes, ϕ_j are the eigenfunctions, and $V_c(y,t)$ is the continuum. The amplitude factors A_j and the frequencies ω_j are in general functions of $\tilde{\gamma}_{\delta^*}$ and Re. Once an initial condition has been prescribed, use of the orthogonality principle between the eigenfunctions and the adjoint eigenfunctions allows the amplitude factors A_j and the continuum V_c to be found. Although this procedure is mathematically correct formally, it is of limited practical use when studying transient behaviour because of the difficulty in the expansion process. Instead, we will carefully solve the system (12) and (13) numerically for a given prescribed initial condition which, by default, will contain both the discrete and the continuum within its solution set.

Before we proceed further, it should be remembered that N, the number of discrete modes, is finite for $\phi < 90^\circ$ and zero for $\phi = 90^\circ$. To show that only a continuum exists, consider a three-dimensional disturbance with $\phi = 90^\circ$ (i.e. $\alpha_{\delta^*} = 0$ and $\tilde{\gamma}_{\delta^*} = \beta_{\delta^*}$). The basic equations, (12) and (13), reduce to

$$\frac{\partial}{\partial t}\left(\frac{\partial^2\check{v}}{\partial y^2} - \beta_{\delta^*}^2\check{v}\right) = R_{\delta^*}^{-1}\left[\frac{\partial^4\check{v}}{\partial y^4} - 2\beta_{\delta^*}^2\frac{\partial^2\check{v}}{\partial y^2} + \beta_{\delta^*}^4\check{v}\right] \tag{21}$$

and

$$\frac{\partial\tilde{w}}{\partial t} = U'\check{v} + R_{\delta^*}^{-1}\left[\frac{\partial^2\tilde{w}}{\partial y^2} - \beta_{\delta^*}^2\tilde{w}\right]. \tag{22}$$

Note that the first equation is independent of the mean flow U. As such, Gustavsson (1979) and Salwen & Grosch (1981) have shown that the solution can be written as

$$\check{v}(y,t) = \int_0^\infty a_k(\beta)\phi_{\beta_{\delta^*}k}(y)\mathrm{e}^{-(\beta_{\delta^*}^2+k^2)t/R_{\delta^*}}\,\mathrm{d}k, \tag{23}$$

where the eigenfunctions are given by

$$\phi_{\beta_{\delta^*}k}(y) = \left(\frac{2}{\pi}\right)^{1/2}\frac{k}{\beta_{\delta^*}^2+k^2}\left[\mathrm{e}^{-|\beta_{\delta^*}|y} - \cos(ky) + |\beta|k^{-1}\sin(ky)\right], \tag{24}$$

and the coefficients are found by applying the initial condition

$$a_k(\beta_{\delta^*}) = \int_0^\infty \check{v}(y,0)\phi_{\beta_{\delta^*}k}(y)\mathrm{d}y. \tag{25}$$

Thus, there are no discrete eigenmodes but rather only a continuum of eigenfunctions. Salwen & Grosch (1981) have also shown that this solution decays in time as

$$\check{v} \approx t^{-1/2}\mathrm{e}^{-\beta_{\delta^*}^2 t/R_{\delta^*}} \quad \text{as} \quad t \to \infty.$$

Several remarks concerning the case $\phi = 90^\circ$ are in order. Since only the continuum

Grid points	Growth rate
500	0.00285574
1000	0.00285181
2000	0.00284947
4000	0.00284961

TABLE 1. The numerically computed growth rate of a two-dimensional Tollmien–Schlichting wave as a function of number of grid points. $Re = 10^3, \tilde{\gamma} = 0.24, \phi = 0$.

solution exists, the Blasius boundary layer is asymptotically stable at all wavenumbers β and at all Reynolds numbers. In all the cases considered here, the normalized growth of $\check{v}$ decays for all time, indicating that the observed transient growth is due entirely to the presence of the forcing term $U'\check{v}$ in the Squire equation. Thus, it is the existence of a continuum of eigenfunctions that produces algebraic instability (defined below) as given by the large transient algebraic growth under these conditions. The argument that it is the non-normality of the linear Orr–Sommerfeld and Squire operators, as might be the case in bounded channel flows, does not apply here.

4. Numerical solutions

The partial differential equations (12) and (13) were solved numerically by the method of lines (see e.g Ames 1977). This choice is a convenient numerical method; other techniques are possible. The spatial derivatives were centre differenced on a uniform grid and the resulting system was then integrated in time by a fourth-order Runge–Kutta scheme. All calculations were done in 64-bit precision. The results were checked for convergence by increasing the number of mesh points. For verification, table 1 shows the numerically computed growth rate of a two-dimensional Tollmien–Schlichting wave as a function of grid points for $Re = 10^3$, $\tilde{\gamma} = 0.24$ and $\phi = 0°$. Growth rates were computed by integrating the equations forward in time beyond the transient until the growth rate, defined as $\omega_i = \ln|E(t)|/2t$ where $|E|$ is the amplitude of the perturbation energy defined below, asymptotes to a constant value.

The value obtained from an Orr–Sommerfeld solver is 0.00284962. No effort was made to optimize the number of grid points by employing non-uniform meshes. If this was done, far fewer grid points would be needed. All calculations presented in this paper used 5000 grid points and thus represent grid-independent solutions.

Before investigating the effects of various initial conditions and their subsequent transient behaviour, it is instructive to compare the numerically computed growth rates to those using the Orr–Sommerfeld equation at supercritical Reynolds numbers. Figure 1(*a*) shows the post-transient growth rates obtained from the numerical solution of (12) (shown as circles) and those obtained from the Orr–Sommerfeld equation (shown as the solid curve) for $Re = 10^3$ and $\phi = 0°$. As expected, the agreement is excellent. To demonstrate the strength of the procedure, figure 1 also shows similar results but at $Re = 10^4$ (*b*) and $Re = 10^5$ (*c*).

5. Perturbation energy

As mentioned above, the effects of various initial conditions and the subsequent transient behaviour at subcritical Reynolds numbers is the major focus of the present study. The energy density in the $(\tilde{\gamma}, \phi)$-plane as a function of time is computed and is

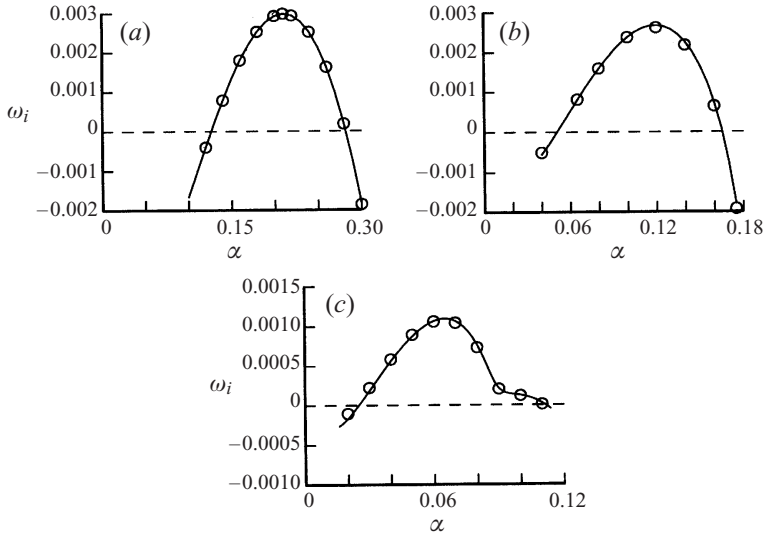

FIGURE 1. Plot of growth rate versus wavenumber for two-dimensional disturbances, $\phi = 0$. Circles represent growth rates calculated by numerical integration, and solid curves are growth rates obtained from the Orr–Sommerfeld equation (normal mode solution). Reynolds numbers: (*a*) $Re = 10^3$, (*b*) $Re = 10^4$, and (*c*) $Re = 10^5$.

defined as

$$E(t;\tilde{\gamma},\phi,Re) = \int_0^\infty \left[|(\breve{u}-\breve{u}_\infty)^2| + |(\breve{v}-\breve{v}_\infty)^2| + |(\breve{w}-\breve{w}_\infty)^2|\right] \mathrm{d}y, \tag{26}$$

where $()_\infty$ denotes values at infinity, which may be a function of time. Note that in using this definition we have allowed for disturbances that are bounded at infinity. The total energy of the perturbation can be found by integrating (26) over all $\tilde{\gamma}$ and ϕ. A growth function can be defined in terms of the normalized energy density, namely

$$G(t;\tilde{\gamma},\phi,Re) = \frac{E(t;\tilde{\gamma},\phi,Re)}{E(0;\tilde{\gamma},\phi,Re)}, \tag{27}$$

that effectively measures the growth of the energy at time t for a prescribed initial condition at $t = 0$. For cases where it is known that the solution is asymptotically stable for large time, we use the bases that, if $G > 1$ for some time $t > 0$, then the flow is said to be algebraically unstable; if $G = 1$ for all time, the flow is algebraically neutral; and, if $G < 1$ for all time, the flow is algebraically stable.

5.1. *Response to a particular initial condition*

We first show selected results for a particular initial condition given by a Gaussian, namely

$$\breve{v} = V_0 \left(\frac{y}{y_0}\right)^2 \mathrm{e}^{-(y-y_0)^2/\sigma}, \qquad \tilde{w} = 0, \tag{28}$$

centred at y_0 with width determined by σ; V_0 can, of course, be a function of $\tilde{\gamma}$ and ϕ. This initial value is chosen so that the boundary conditions at $y = 0$ are satisfied. Figure 2(*a*) is a plot of the normalized energy $G(t)$ for $\tilde{\gamma} = 0.24$, $\phi = 0°$, $Re = 10^3$, $\sigma = 0.25$ and for various values of y_0. From this plot we see that for each value of y_0, the perturbation energy grows exponentially in accordance with

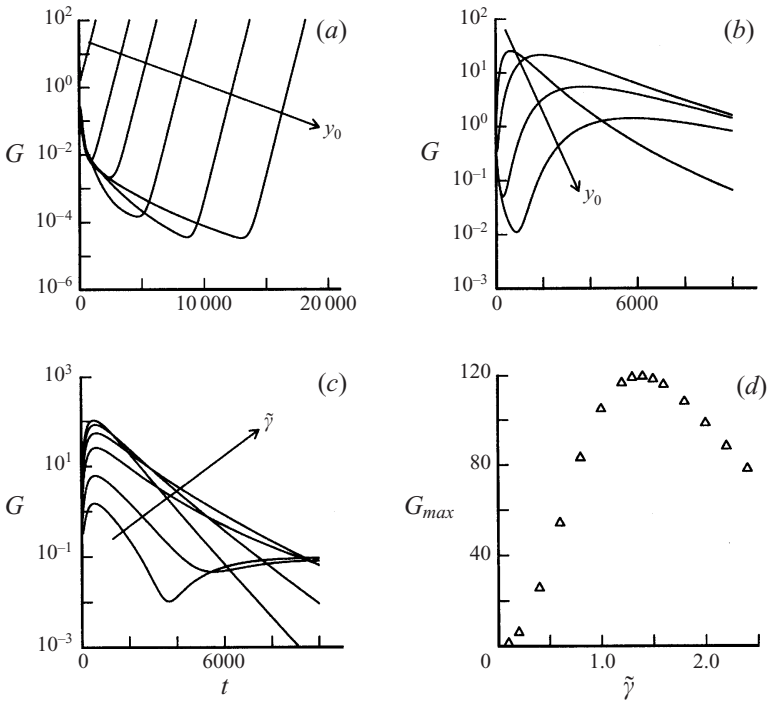

FIGURE 2 (*a–c*). Normalized energy G versus time using initial condition (28) with $Re = 10^3$ and $\sigma = 0.25$. (*a*) $\tilde{\gamma} = 0.24$, $\phi = 0°$, and $y_0 = 2, 4, 6, 8, 10, 12$, (*b*) $\tilde{\gamma} = 0.4$, $\phi = 90°$, and $y_0 = 2, 4, 5, 6, 7, 8$; and (*c*) $\tilde{\gamma} = 0.1, 0.2, 0.4, 0.6, 0.8, 1.0$, $\phi = 90°$, and $y_0 = 2$. (*d*) Maximum over time of normalized energy G versus wavenumber with $Re = 10^3$ and $\sigma = 0.25$; $\phi = 90°$ and $y_0 = 2$.

classical stability theory. However, the time at which the eventual exponential growth is initiated depends on the location of the Gaussian initial condition. That is, as the location moves further out of the boundary layer (recall that the boundary layer edge is at $y \approx 5$), the time at which exponential growth occurs also increases. What might not be expected is that even for $y_0 = 8$, which lies outside the boundary layer, a Tollmien–Schlichting wave is still generated. This can be explained by appealing to the general solution given by (20). Since any solution can be expanded in terms of the discrete modes and the continuum and since the initial condition is not entirely contained within the continuum, there must be a non-zero coefficient for all discrete modes. The non-zero coefficient for the unstable discrete mode, no matter how small, eventually gives rise to the observed exponential growth shown in figure 2(*a*). This observation is also noted and discussed in the work of Hill (1995), which should be reviewed for more details. And, more importantly, this point can be completely missed if one ignores the effect of initial conditions and instead relies entirely on the classical stability framework. This revelation is important and could have critical consequences in the areas of receptivity and flow control and will be the subject of future investigations.

Also shown are results for $\phi = 90°$ (figure 2*b*). Recall that at this angle only the continuum exists and there are no normal modes. In this case, increasing the location of the Gaussian y_0 results in a decrease in the maxima of the perturbation energy. In figure 2(*c*) we show the effect of varying $\tilde{\gamma}$ for $\phi = 90°$ and with $y_0 = 2$. Note that the maximum of G increases with increasing $\tilde{\gamma}$. However, as shown in figure 2(*d*) where

the maximum of G in time (denoted by G_{max}) for a given fixed wavenumber is shown, the maximum does not increase without bound. The largest value of $G_{max} = 119.6$ occurs for $\tilde{\gamma} = 1.4$. The idea of determining the largest possible value of G_{max} for a set of initial conditions is explored in the next section.

5.2. *Optimal initial conditions*

Since the strong amplification of disturbances during the initial period has been proposed as a mechanism for bypass transition, it is worthwhile to ascertain what the maximum growth may be during this period and whether such growth is to be expected from arbitrary disturbances or whether the disturbance must have special properties to achieve the maximum growth. For the problem of bounded channel flow, Criminale *et al.* (1997) showed that a set of functions different from the (non-orthogonal) eigenfunctions can be readily employed to answer such a question. That technique is appropriately modified here to investigate the maximum transient growth allowed by the linearized Navier–Stokes equations. We start by considering disturbances with only spanwise vorticity initially and then proceed to disturbances in which an initial normal vorticity is included. Although these two types of disturbances do indeed evolve independently in the linear regime, it is the combined response that determines whether or not the overall growth is such that it violates the assumptions of linearity. Thus if very large relative growth is achieved in one mode, it does not necessarily mean that a very large relative growth will be achieved when the two modes are combined appropriately.

To start the optimization scheme, we consider the total solution $\boldsymbol{u} = (\breve{u}, \breve{v}, \breve{w})$ to be the sum

$$\boldsymbol{u}(y,t) = \sum_{k=1}^{N} (a_k + \mathrm{i}b_k)\boldsymbol{u}_k(y,t), \tag{29}$$

with each of the vectors $\boldsymbol{u}_k(y,t)$ representing a solution to equations (12) and (13) subject to the initial conditions

$$\boldsymbol{u}(y,0) = \begin{cases} \cos\phi\, \partial\breve{v}_k/\partial y \\ \mathrm{i}\tilde{\gamma}\, \breve{v}_k \\ \sin\phi\, \partial\breve{v}_k/\partial y \end{cases} \tag{30}$$

where $\breve{v}_k(0,t)$ are some set of functions defined below. In order to maximize the growth function, it is sufficient to maximize the energy,

$$E(t) = \int_0^\infty (\boldsymbol{u}(y,t) - \boldsymbol{u}_\infty) \cdot (\boldsymbol{u}^*(y,t) - \boldsymbol{u}^*_\infty)\, \mathrm{d}y \tag{31}$$

subject to the constraint

$$E(0) = 1.$$

Therefore, using Lagrange multipliers to maximize the function

$$\bar{G}(t) = \int_0^\infty (\boldsymbol{u}(y,t) - \boldsymbol{u}_\infty) \cdot (\boldsymbol{u}^*(y,t) - \boldsymbol{u}^*_\infty)\, \mathrm{d}y - \lambda \left(\int_0^\infty (\boldsymbol{u}(y,0) - \boldsymbol{u}_\infty) \cdot (\boldsymbol{u}^*(y,0) - \boldsymbol{u}^*_\infty)\, \mathrm{d}y - 1 \right), \tag{32}$$

requires

$$\frac{\partial \bar{G}}{\partial a_k} = 0, \qquad \frac{\partial \bar{G}}{\partial b_k} = 0, \qquad k = 1, 2, \cdots, N.$$

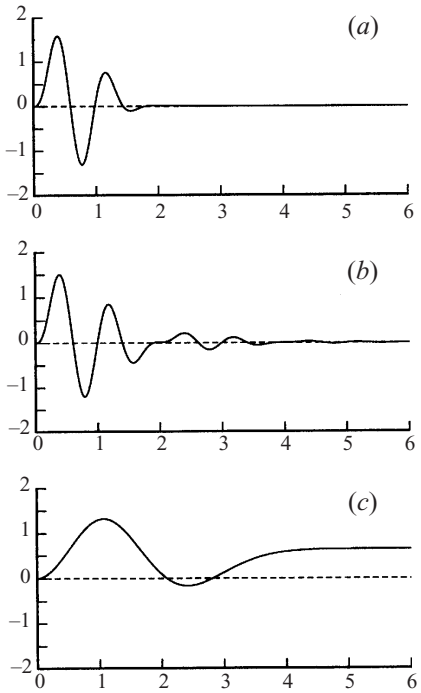

FIGURE 3. Third orthogonal function: (*a*) Subspace 1, (*b*) Subspace 2, (*c*) Subspace 3.

The set of equations thus derived results in a $2N \times 2N$ generalized eigenvalue problem. A search over the eigenvectors gives the initial condition with initial unit energy that maximizes the function $\bar{G}$ at time t.

Various initial conditions are used to explore transient behaviour at subcritical and supercritical Reynolds numbers. Since only a finite number of normal modes exists for the boundary layer, there does not exist a complete discrete set of orthogonal functions, square integrable over $(0, \infty)$ in the sense of (26) with the function and its first derivative zero at the plate that can completely describe all possible initial conditions. For this reason we shall consider three subspaces that satisfy the boundary condition (14) at the plate and have different characteristics at infinity.

The first subspace is spanned by the set of functions

$$v_n = \left[y - \frac{\sin(n\pi y)}{n\pi} \right] \mathrm{e}^{-y^2}, \qquad n = 1, 2, 3, \cdots, \tag{33}$$

which decay rapidly to zero at infinity. This subspace is chosen to represent disturbances that are non-zero inside the boundary layer and essentially zero outside the boundary layer.

The second subspace is spanned by the set of functions

$$v_n = \left[y - \frac{\sin(n\pi y)}{n\pi} \right] \mathrm{e}^{-y}, \quad n = 1, 2, 3, \cdots, \tag{34}$$

is similar to the first subspace except that the functions decay more slowly as $y \to \infty$. This subspace is chosen to represent disturbances which are non-zero inside the boundary layer and at the edge of the boundary layer. The set of functions defined by the bracket term are known as the Figer functions.

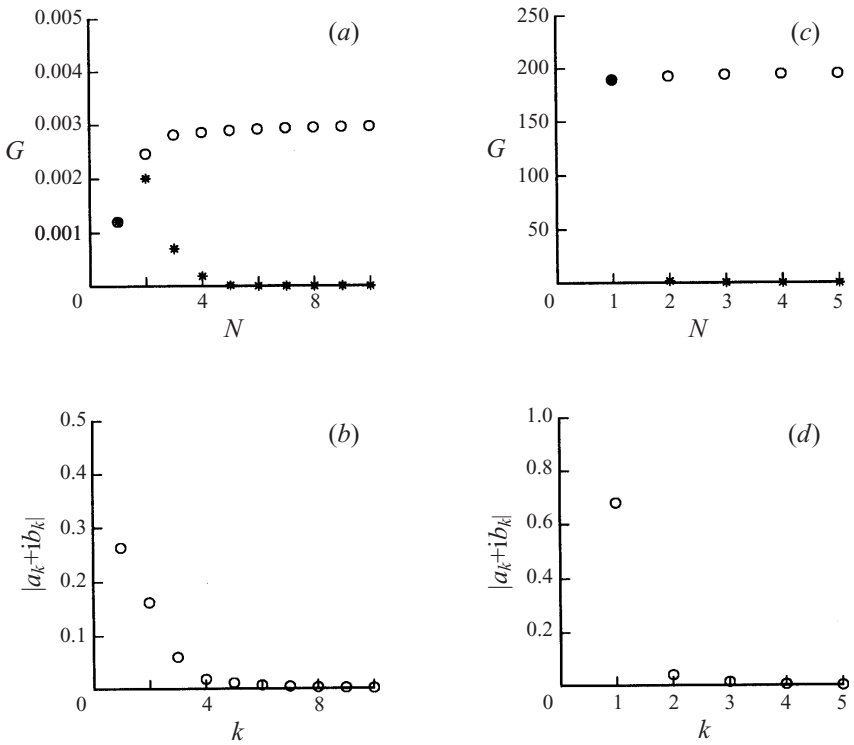

FIGURE 4. (*a*) Normalized energy function G versus mode number N at $t = 65$ using subspace 2 as initial conditions. Asterisks for individual modes, circles for optimization using N modes. $Re = 600$, $\tilde{\gamma} = 0.9$, and $\phi = 0°$ (*b*) Magnitude of optimal coefficients for (*a*) with $N = 10$. (*C*) Same as (*a*) with $t = 200$ and $\phi = 90°$. (*d*) Magnitude of optimal coefficients for (*a*) with $N = 5$.

The third subspace is spanned by the set of functions

$$v_i = \int_0^y H_i(\bar{y}) \mathrm{e}^{-\bar{y}^2/2} \, \mathrm{d}\bar{y}, \quad i = 1, 3, 5, \cdots, \tag{35}$$

where H_i are the Hermite polynomials. Only the odd Hermite polynomials are taken since they vanish at the plate. This set is only bounded at infinity and thus explores disturbances which are non-zero in the free stream.

From each subspace, an orthonormal set for the initial condition $\{\check{v}_n(u, 0), \ n = 1, 2, \ldots\}$ is created by the Gram–Schmidt process. The third function from each orthonormal set is shown in figure 3.

For the integration of (13) the initial condition $\tilde{w} = 0$ is chosen for the results presented below. In a separate subsection we shall relax this last initial condition and examine the effect of initial normal vorticity on the growth of the perturbation energy density.

5.2.1. *Zero initial normal vorticity*

To illustrate the optimization procedure, we first perform the calculations for the following two cases using the initial conditions as specified by subspace 2. The first is the computation of a optimal two-dimensional initial conditions for $\tilde{\gamma} = 0.9$, $\phi = 0°$ and $Re = 600$ (discrete stable modes). In figure 4(*a*) we show the growth factor at $t = 65$ for each individual mode as well as for the optimal solution for various values

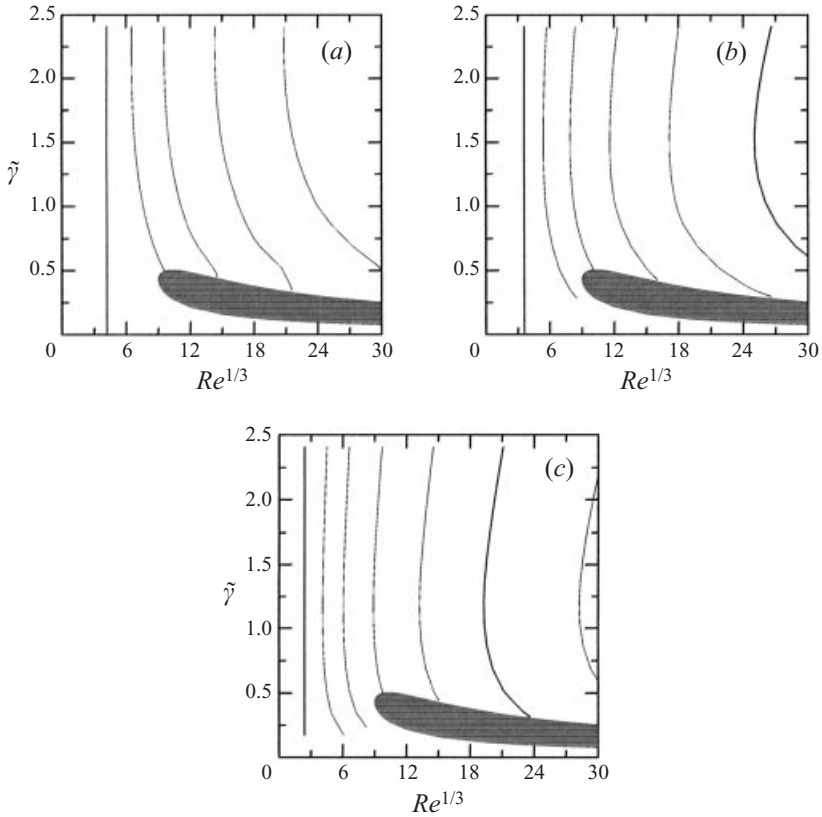

FIGURE 5. Optimized maximum of normalized energy function G over time. Values of G for each contour from left to right: 10^0, 10^1, $10^2, \ldots, 10^7$. (*a*) Subspace 1, (*b*) Subspace 2, and (*c*) Subspace 3.

of N. Note the rapid convergence as $N \to \infty$. In figure 4(*b*) the magnitudes of the coefficients which produce the optimum with $N = 10$ are shown. The contribution from the higher modes does not significantly affect the optimal initial conditions. The second calculation is for an optimal three-dimensional disturbance. The parameters chosen are $Re = 600$, $\tilde{\gamma} = 0.9$ and $\phi = 90^\circ$ (no discrete modes). The results are shown in figure 4(*c*) and Figure 4(*d*) at $t = 200$. Both plots illustrate the advantage of using orthogonal functions for the initial conditions in that the first few modes display almost entirely the optimal solution, while the magnitudes of the coefficients of the optimal solution are bounded above by one and decay rapidly to zero.

The results presented above determine the maximum of G at a particular time and do not determine the maximum of G for all time. Consequently, results for the global optimum in the $(\tilde{\gamma}, Re)$-plane for three-dimensional disturbances are discussed next. At each Reynolds number, and at each value of $0 < \tilde{\gamma} < 1.4$, the global maximum of G over time is found and denoted by G_{opt}. Contour plots of G_{opt} are then constructed in the $(\tilde{\gamma}, Re)$-plane. Figure 5 shows the global optimum for each of the three subspaces. Also shown is the unstable region (shaded) for two-dimensional normal modes as computed from the Orr–Sommerfeld equation. For a given subcritical Reynolds number, disturbances from subspace 3 that are non-zero in the free stream allow greater transient growth than disturbances from subspace 1 and subspace 2 which decay rapidly in the free stream (compare figure 5*c* to figure 5*a* and figure 5*b*).

To further illustrate the differences between the three subspaces, figure 6(*a*) shows the optimal growth function G against time for $\phi = 90°$, $Re = 10^3$ and $\tilde{\gamma} = 0.65$. These values were chosen so as to compare with the results of Butler & Farrell (1992) where it was shown that the global optimal $G_{opt} = 1514$ for a three-dimensional disturbance at $Re = 10^3$ occurs for $\tilde{\gamma} = 0.65$ at $t = 778\sqrt{2}$. The global optima determined here are as follows: for subspace 1, $G_{opt} = 20.4$; for subspace 2, $G_{opt} = 157.4$; and for subspace 3, $G_{opt} = 1472.1$. Clearly, the growth is smaller for disturbances confined within the boundary layer as compared to the growth for disturbances which are bounded at infinity. Indeed, using only the first mode for subspace 3 produces about 93% of the optimum growth reported by Butler & Farrell using only an approximation to a true continuum for their boundary layer calculations. This is a strong indication that in any bypass transition mechanism that is proposed, the effects of the continuum must to be considered.

5.2.2. *Non-zero initial normal vorticity*

Since the large transient growth presented above for three-dimensional disturbances is a direct result of the growth of normal vorticity, it is necessary to ask whether the growth is a special case caused by neglecting the initial normal vorticity or will the growth in energy remain once the energy of non-zero initial normal vorticity is included in the calculation. Therefore, we present the results for three different initial specifications of $\tilde{w}$, namely

$$\begin{aligned} \text{CASE I:} \quad & \tilde{w} = 0 \\ \text{CASE II:} \quad & \tilde{w} = Ay\mathrm{e}^{-y}, \\ \text{CASE III:} \quad & \tilde{w} = Ay\mathrm{e}^{-y^2}. \end{aligned}$$

Each case satisfies the no-slip boundary condition at the plate. The first case has already been discussed above and is repeated here for comparison purposes. The other two cases differ in their decay rates at infinity. The initial condition for $\check{v}$ is chosen to be the first mode of subspace 3 which produces near-optimal transient growth. Figure 6(*b*) shows the normalized perturbation energy G as a function of time for each of the three cases with $\tilde{\gamma} = 0.65$, $Re = 10^3$, $\phi = 90°$ with $A = 1$ and $A = 10$. The results suggest that algebraic growth, as measured here, is sensitive to the presence of any initial normal vorticity, specifically to the inclusion of the energy associated with the initial normal vorticity in the normalization of the growth factor. The transient growth is significantly reduced when $A = 10$. If the amplitude A is increased further, the flow would become algebraically stable. This effect is shown for initial conditions that produce near-optimal transient growth. For initial disturbances confined to the boundary layer, the effect of non-zero initial normal vorticity is even more dramatic and a much lower value of the amplitude A is necessary for the flow to become algebraically stable. This phenomenon is discussed further in the next section.

6. Analytical evaluation of the early period

It is always desirable, if possible, to have some form of an analytical solution to a problem that has been solved numerically. Then, as questions arise about the solution, an alternative approach is available to help gain additional insight. The details and the procedure needed to examine the initial-value problem for the boundary layer, as presented here, have been provided by Grosch & Salwen (1978) and Salwen & Grosch (1981). These works employ the traditional modal approach, i.e. travelling-

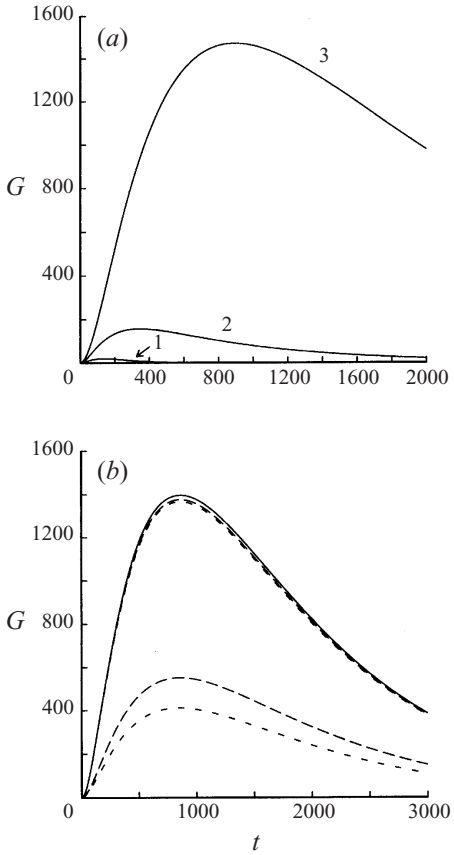

FIGURE 6. (*a*) Normalized energy function G versus time for optimal initial conditions: (1) subspace l, (2) subspace 2, and (3) subspace 3. $Re = 10^3$, $\tilde{\gamma} = 0.65$, and $\phi = 90^\circ$ corresponding to the case of Butler & Farrell (1992). (*b*) Plot of normalized energy function G versus time for zero and non zero initial normal vorticity. $Re = 10^3$, $\tilde{\gamma} = 0.65$, and $\phi = 90^\circ$. Largest growth for case I; larger dashes for case II with $A = 1$ and $A = 10$; and smaller dashes for case III with $A = 1$ and $A = 10$.

wave solutions are used as the means of reducing the partial differential equation to the Orr–Sommerfeld ordinary differential equation. A thorough discussion of the eigenvalues and expansions of arbitrary functions in terms of the eigenfunctions ensues with particular emphasis given to the existence of a continuous spectrum in addition to the more familiar discrete spectrum. Even though this work clearly provides the essential elements, difficulties remain when actually performing the tasks required and they are made even more intractable by the inclusion of the role of three-dimensionality. Still, the importance of these works cannot be under emphasized. Since there are only a finite number of discrete eigenmodes for the boundary layer (Mack 1976), with the number depending upon the value of the Reynolds number, it is clear that no arbitrary initial-value calculation can be made without the addition of the continuous spectrum and the early period dynamics are closely tied to the contribution of the continuous spectrum.

In determining an analytical solution for perturbations in parallel shear flow, often the starting point is to consider the prototypical governing equations known as the Orr–Sommerfeld and the Squire equations. In this system, even when investigating the full three-dimensional problem, the first of these equations is completely uncoupled

and is only fourth order. Hence, the second equation must be second order and contains an inhomogeneous term due to the interaction of the solutions of the Orr–Sommerfeld part of the system with the mean flow. This inhomogeneity, known as vortex tilting, indicates a possibility for resonance when using the conventional modal form of travelling waves for solving the partial differential equations. This point has been exploited by Gustavsson (1979) and Gustavsson & Hultgren (1980) for channel flows while Benney & Gustavsson (1981) considered the case of the boundary layer. In channel flow, such a resonance with damped modes was shown to be possible, thus creating the possibility of temporal behaviour that is algebraic. The numerical calculations of Gustavsson & Benney indicate, however, that direct resonance between discrete modes does not occur in the boundary layer. As a result, the only bases for algebraic behaviour in the boundary layer must rest with (*a*) the additional continuous spectrum and (*b*) the fact that the differential equations are not self-adjoint (Reddy & Henningson 1993; Trefethen *et al.* 1993, among others).

It should be emphasized that it is the transient period of the dynamics that is the central issue. There are no conflicts or difficulties with the asymptotic fate of disturbances because any growing normal mode will dominate (in the unstable regions) as time gets large. In this sense, very few modes need be computed to obtain such knowledge. In fact, for the boundary layer there is only one amplified mode in the discrete spectrum with all the rest damped for most Reynolds numbers (assuming a solid wall). However, for an initial-value problem, inclusion of the damped modes is critical for an arbitrary specification. The use of Laplace transforms in time to reduce the system to ordinary differential equations and the same eigenvalue problem is an alternative that has been used by Gustavsson (1979) and Hultgren & Gustavsson (1980). When done, it shows that the normal modes are those corresponding to poles in the complex plane with a branch cut providing the continuous spectrum. Unfortunately, even though this approach captures all essentials of the mathematics, one is still left with the same basic differential equations that must be solved for an initial-value calculation. Also, because of the inability to obtain any closed form representation, a thorough assessment of details is difficult to obtain.

The works of Criminale & Drazin (1990, 1998) suggest alternative means to that of the travelling wave hypothesis for examining a very general solution to the initial-value problem (in fact, exact solutions to the full Navier–Stokes equations), but it is limited to mean profiles that vary only linearly in the relevant independent variable (constant shear). Thus, although important observations are possible using such an approach, any effects that are due to a continuously varying mean profile that solve the mean flow equations are lost when using this scheme.

The numerical schemes used here for solving the partial differential equations directly circumvent many of the difficulties of normal mode analysis and are not limited to linear profiles as is the work of Criminale & Drazin. Still, it would be beneficial if this work could be supplemented with some analysis; one such means is suggested here.

We find it enlightening to use the moving coordinate transformation that was employed by Criminale & Drazin (1990, 1997) in order to solve the linear partial differential equations. Thus, let

$$T = t, \qquad \xi = x - U(y)t, \qquad \eta = y, \qquad \text{and} \qquad \zeta = z. \tag{36}$$

This change of variables is not the well known shift from an Eulerian to a Lagrangian frame of reference but it does provide a means of simplifying and evaluating the early-time behaviour analytically. The governing equations in terms of the vertical

component of the perturbation velocity, v, and the normal perturbation vorticity, $\omega_y = \partial u/\partial z - \partial w/\partial x$, become

$$\frac{\partial \nabla^2 v}{\partial T} - \frac{\mathrm{d}^2 U}{\mathrm{d}\eta^2}\frac{\partial v}{\partial \xi} = \epsilon \nabla^2 \nabla^2 v \tag{37}$$

and

$$\frac{\partial \omega_y}{\partial T} - \epsilon \nabla^2 \omega_y = \frac{\mathrm{d}U}{\mathrm{d}\eta}\frac{\partial v}{\partial \zeta} \tag{38}$$

with

$$\nabla^2 = \frac{\partial^2}{\partial \xi^2} + \frac{\partial^2}{\partial \eta^2} + \frac{\partial^2}{\partial \zeta^2} + T^2\left(\frac{\mathrm{d}U}{\mathrm{d}\eta}\right)^2 \frac{\partial^2}{\partial \xi^2} - 2T\frac{\mathrm{d}U}{\mathrm{d}\eta}\frac{\partial^2}{\partial \eta \partial \xi} - T\frac{\mathrm{d}^2 U}{\mathrm{d}\eta^2}\frac{\partial}{\partial \xi},$$

and $\epsilon = R_{\delta^*}^{-1}$.

A Fourier decomposition in the new variables ξ, ζ is taken, thus reducing the problem to the initial-value, boundary-value scenario that is traditional except that the ξ, ζ variables are not the same as x, z and the equations remain partial differential equations.

In terms of the new variables the Fourier transform is given by

$$\check{v}(\alpha, \eta, \beta, T) = \int_{-\infty}^{+\infty}\int_{-\infty}^{+\infty} v(\xi, \eta, \zeta, T)\mathrm{e}^{\mathrm{i}(\alpha\xi + \beta\zeta)}\mathrm{d}\xi\mathrm{d}\zeta, \tag{39}$$

and the governing equations can be written as

$$\frac{\partial \Delta \check{v}}{\partial T} + \mathrm{i}\tilde{\gamma}\cos\phi\frac{\mathrm{d}^2 U}{\mathrm{d}\eta^2}\check{v} = \epsilon\Delta\Delta\check{v} \tag{40}$$

and

$$\frac{\partial \tilde{w}}{\partial T} - \epsilon\Delta\tilde{w} = \sin\phi\frac{\mathrm{d}U}{\mathrm{d}\eta}\check{v} \tag{41}$$

where

$$\check{\omega}_y = \mathrm{i}\tilde{\gamma}\tilde{w}, \qquad \tilde{\gamma}^2 = \alpha^2 + \beta^2, \qquad \text{and} \qquad \tan\phi = \beta/\alpha \tag{42}$$

have been used. The Laplacian in the new variables is

$$\Delta = \frac{\partial^2}{\partial \eta^2} + \mathrm{i}2\tilde{\gamma}\cos\phi T\frac{\mathrm{d}U}{\mathrm{d}\eta}\frac{\partial}{\partial \eta} - \tilde{\gamma}^2 - \tilde{\gamma}^2 T^2\cos^2\phi\left(\frac{\mathrm{d}U}{\mathrm{d}\eta}\right)^2 + \mathrm{i}\tilde{\gamma}\cos\phi T\frac{\mathrm{d}^2 U}{\mathrm{d}\eta^2}. \tag{43}$$

Solutions of this set of equations must be solved subject to the boundary conditions

$$\check{v} = \frac{\partial \check{v}}{\partial \eta} = \tilde{w} = 0 \quad \text{at } \eta = 0 \tag{44}$$

and $\check{v}$, v_η, and $\tilde{w}$ bounded as $\eta \to \infty$.

The shift to the moving coordinates suggests at least one means for investigating details of an initial-value problem under arbitrary specifications. For example, in this frame of reference it can be seen that there is mathematically no critical layer that is so common to normal modes. This observation removes one difficulty, but it remains a singular perturbation problem in the limit $\epsilon \to 0$. However, from numerical work, it is known that much of the relevant behaviour that is under investigation here is found for small values of the polar wavenumber, $\tilde{\gamma}$. In addition, this parameter range includes the region of instability. Thus it is reasonable that the polar wavenumber can be exploited as a small parameter rather than ϵ. By accepting this as a basis,

the problem is changed from a singular to one of a regular perturbation expansion. Moreover, a solution to the partial differential equations can be found directly. One criticism of this approach is that the solution will be valid only for small to order-one values of time, owing to the presence of the products of $\tilde{\gamma}T$ in the governing equations. However, the region of validity is exactly the time regime that is of such importance to resolve and is the most difficult to analyse with a modal approach. This approach is not without its difficulties; care must be taken in order to satisfy the conditions at infinity and all of the details will be provided below. One major result of using this approach is that the sensitivity of the energy growth to the inclusion of non-zero initial normal vorticity is readily explained.

To proceed with the analysis, assume that $\tilde{\gamma} \ll 1$ and that the dependent variables are expanded in a perturbation series as

$$\check{v} = \check{v}_0 + \tilde{\gamma}\check{v}_1 + \tilde{\gamma}^2\check{v}_2 + \ldots, \quad \tilde{w} = \tilde{w}_0 + \tilde{\gamma}\tilde{w}_1 + \tilde{\gamma}^2\tilde{w}_2 + \ldots\ . \tag{45}$$

In a similar manner the operator, Δ, is written as

$$\Delta = \Delta_0 + \tilde{\gamma}\Delta_1 + \tilde{\gamma}^2\Delta_2 \tag{46}$$

with

$$\Delta_0 = \frac{\partial^2}{\partial\eta^2},\ \Delta_1 = \mathrm{i}\cos\phi T\left(2\frac{\mathrm{d}U}{\mathrm{d}\eta}\frac{\partial}{\partial\eta} + \frac{d^2U}{\mathrm{d}\eta^2}\right), \quad \text{and } \Delta_2 = -\left[1 + \cos^2\phi T^2\left(\frac{\mathrm{d}U}{\mathrm{d}\eta}\right)^2\right]. \tag{47}$$

After substituting (45)–(47) into equations (40) and (41) and collecting terms of equal order, the sequence becomes for $O(1)$:

$$\frac{\partial}{\partial T}\Delta_0\check{v}_0 = \epsilon\Delta_0\Delta_0\check{v}_0, \tag{48}$$

$$\frac{\partial\tilde{w}_0}{\partial T} - \epsilon\Delta_0\tilde{w}_0 = \sin\phi\frac{\mathrm{d}U}{\mathrm{d}\eta}\check{v}_0; \tag{49}$$

and for $O(\tilde{\gamma})$:

$$\frac{\partial\Delta_0\check{v}_1}{\partial T} - \epsilon\Delta_0\Delta_0\check{v}_1 = -\mathrm{i}\cos\phi\frac{\mathrm{d}^2U}{\mathrm{d}\eta^2}\check{v}_0 - \frac{\partial}{\partial T}\Delta_1\check{v}_0 + \epsilon[(\Delta_0\Delta_1 + \Delta_1\Delta_0)\check{v}_0]. \tag{50}$$

$$\frac{\partial\tilde{w}_1}{\partial T} - \epsilon\Delta_0\tilde{w}_1 = \sin\varphi\frac{\mathrm{d}U}{\mathrm{d}\eta}\check{v}_1 + \epsilon\Delta_1\tilde{w}_0. \tag{51}$$

The problem requires an initial specification. In the previous sections, an initial normal velocity was specified. This was really just a matter of mathematical and computational convenience. All choices were consistent with the proper choice of an initial specification which is in terms of an initial vorticity (Salwen & Grosch 1981). By examining the physics, this is indeed found to be reasonable. The laminar boundary layer (*per se*) is created by the sudden input of vorticity at the leading edge and the subsequent flow then becomes a balance between the advection of the vorticity downstream with the diffusion in the direction normal to the flat plate. And, for the basic problem, there is only the one component of the vorticity in the z-direction. It is thus convenient to put the perturbation problem on the same basis by specifying the vorticity at time $t = 0$. That this is mathematically proper can be seen by noting that, although the two governing equations are presented in terms of the velocity components, these equations are actually those governing the perturbation

vorticity and are obtained by eliminating the pressure. Indeed, the Squire equation directly governs the normal vorticity component. Furthermore, by using the moving coordinates and the Fourier transforms, the expression

$$\nabla^2 v = \frac{\partial \omega_z}{\partial x} - \frac{\partial \omega_x}{\partial z} \tag{52}$$

becomes

$$\Delta\check{v} = \mathrm{i}\tilde{\gamma}(\sin\phi\check{\omega}_x - \cos\phi\check{\omega}_z).$$

Thus, in wave space, $\Delta\check{v}$ is proportional to the vorticity components in the plane perpendicular to $\check{\omega}_y$. The most general initial conditions can thus be represented by two independent modes of vorticity:

$$\Delta\check{v} = \mathrm{i}\tilde{\gamma}\Omega_t(\tilde{\gamma}, \eta, \phi), \qquad \tilde{w} = 0 \tag{53}$$

and

$$\Delta\check{v} = 0, \qquad \tilde{w} = \frac{\Omega_n(\tilde{\gamma}, \eta, \phi)}{\mathrm{i}\tilde{\gamma}}. \tag{54}$$

A further kinematic constraint that the initial vorticity be solenoidal implies that the former condition has no initial normal vorticity component, whereas the latter condition does indeed have an initial tangential component of vorticity, but it is perpendicular to the initial tangential vorticity represented by the former condition. The solution to the latter vorticity mode requires only the solution to the Squire equation.

In considering the scalings in $\tilde{\gamma}$ for the initial vorticity, it has been assumed that the actual vorticity components ω_x and ω_z are of order one. Thus, it is noted that Ω_t must be an $O(1)$ quantity while Ω_n must be $O(\tilde{\gamma})$ which is the same as specifying $\tilde{w}$ as $O(1)$.

By using the above relation and the definitions for the series expansions and assuming that Ω_t can also be expanded in an appropriate power series, then

$$\Delta_0\check{v}_0 = 0 \qquad \text{and} \qquad \Delta_0\check{v}_1 = \Omega_t^0(\eta, \phi) \tag{55}$$

become the initial conditions for the first of the two governing equations.

It can be seen that the only solution for $\check{v}_0$ that meets the boundary conditions with no input initially is $\check{v}_0 \equiv 0$. Then, moving to $O(\tilde{\gamma})$, the homogeneous partial differential equation

$$\frac{\partial}{\partial T}\left(\frac{\partial^2\check{v}_1}{\partial\eta^2}\right) - \epsilon\frac{\partial}{\partial\eta^2}\left(\frac{\partial^2\check{v}_1}{\partial\eta^2}\right) = 0 \tag{56}$$

must be solved for $\check{v}_1$.

To proceed, some assumption must be made about the specification of $\Omega_t(\tilde{\gamma}, \eta, \phi)$. While it is desired that this initial specification should, in some sense, be allowed to be completely arbitrary, it is determined that the nature of the conditions that must be met by the normal velocity impose certain restrictions on $\Omega_t(\tilde{\gamma}, \eta, \phi)$ (see Lighthill 1963). Fortunately, these restrictions can still be met while allowing for the appropriate degree of arbitrariness. If it is assumed that the leading order of the initial vorticity decays sufficiently as $\eta \to \infty$ then Ω_t can be formally written as either a Fourier cosine or a Fourier sine integral. If the latter is chosen, then the diffusion equation for $v_{1\eta\eta}$ can be solved subject to the specified initial condition. However, the Fourier sine integral implies that there is no vorticity at the wall which is certainly unphysical since the wall is a source of vorticity.

Conversely, if the initial condition is written as the Fourier cosine integral,

$$\Delta_0 \check{v}_1|_{T=0} = \Omega_t^0(\eta, \phi) = \frac{2}{\pi}\int_0^\infty \bar{\Omega}_t^0(\beta)\cos\beta\eta\,\mathrm{d}\beta \tag{57}$$

at time $T = 0$, then this choice is consistent with a small-$\tilde{\gamma}$ expansion of the pressure equation that requires that

$$\frac{\partial^3 \check{v}}{\partial \eta^3} \sim O(\tilde{\gamma}^2). \tag{58}$$

We note that allowing $\bar{\Omega}_t^0(\beta)$ to depend on ϕ will not change the analysis. Thus, it is determined that

$$\frac{\partial^2 \check{v}_1}{\partial \eta^2} = \frac{2}{\pi}\int_0^\infty \bar{\Omega}_t^0(\beta)\mathrm{e}^{-\epsilon\beta^2 T}\cos\beta\eta\,\mathrm{d}\beta \tag{59}$$

for all time. A single integration in η introduces a pole at $\beta = 0$ which implies a non-zero value of $v_{1\eta}$ in the far field at time $T = 0$. The only way to satisfy both $v_{1\eta} = 0$ at $\eta = 0$ and $v_{1\eta} \to 0$ as $\eta \to \infty$ for all time is to require that

$$\bar{\Omega}_t^0(0) = 0. \tag{60}$$

This additional requirement on the initial specification seems to violate the spirit of seeking a solution subject to an arbitrary initial specification; however, for a given arbitrary function $F(\eta)$, a consistent initial specification of vorticity can be found as

$$\Omega_t^0(\eta) = F(\eta) - \int_0^\infty F(\hat{\eta})\,\mathrm{d}\hat{\eta}\,\delta(\eta) \tag{61}$$

where it follows that

$$\bar{\Omega}_t^0(\beta) = \bar{F}(\beta) - \bar{F}(0). \tag{62}$$

From this, it is seen that the wall does indeed act as a source of vorticity as it should. With the issue of the initial specification resolved, the integral representations of the solution are found to be

$$\frac{\partial \check{v}_1}{\partial \eta} = \frac{2}{\pi}\int_0^\infty \bar{\Omega}_t^0(\beta)\mathrm{e}^{-\epsilon\beta^2 T}\frac{\sin\beta\eta}{\beta}\,\mathrm{d}\beta \tag{63}$$

and

$$\check{v}_1 = \frac{2}{\pi}\int_0^\infty \bar{\Omega}_t^0(\beta)\mathrm{e}^{-\epsilon\beta^2 T}\frac{(1-\cos\beta\eta)}{\beta^2}\,\mathrm{d}\beta. \tag{64}$$

From this result, it can be determined that

$$\check{v}_1 = \frac{2}{\pi}\int_0^\infty \frac{\bar{\Omega}_t^0(\beta)\mathrm{e}^{-\epsilon\beta^2 T}}{\beta^2}\,\mathrm{d}\beta \tag{65}$$

as $\eta \to \infty$. Thus, it is seen that the leading-order solution might have a non-zero normal velocity in the free stream. This also implies that the vorticity is a non-zero, $O(\tilde{\gamma}^2)$ quantity in the free stream. Again, this does not seem to allow for the appropriate degree of arbitrariness in the specification of the initial vorticity. However, by considering the solution to depend on more than one length and time scale, it is possible to find a solution to the problem where the initial vorticity decays in the free stream.

In considering the solution to the normal vorticity (the Squire mode) induced by three-dimensional effects, it is clear that the mean velocity must now be incorporated for the first time. In particular, $U'(\eta)$ is required. The traditional representation for

the Blasius profile is not easily suited to this task and therefore a substitution will be used. For this purpose, the exponential series provides an excellent basis for the development of an analytical solution. Thus, consider the exponential series

$$U(\eta) = 1 - a\mathrm{e}^{-\sigma\eta} - b\mathrm{e}^{-2\sigma\eta} - c\mathrm{e}^{-3\sigma\eta} - d\mathrm{e}^{-4\sigma\eta} - \ldots, \tag{66}$$

where $\sigma = U'(0) \equiv 0.33206$ is the value of the shear determined from the Blasius profile. For purposes of comparison, an eigenvalue computation should be made to determine the differences resulting from this profile and that of Blasius. As the number of terms retained in the series increases the accuracy in the numerical value of the eigenvalue improves, but there is not a corresponding improvement in qualitative features of the flow. It is determined that three to four terms are adequate for most of the essentials. On the other hand, the use of the full series is not necessary for the analytical evaluation of the equations because they are linear. Indeed, one exponential term will provide an adequate basis for assessing the initial period of the dynamics. Incorporating more terms of the mean flow series can be done by inference. After making the substitutions and noting the results for $\check{v}_0$ and $\check{v}_1$, the equation to be solved becomes

$$\frac{\partial\tilde{w}_1}{\partial T} - \epsilon\frac{\partial^2\tilde{w}_1}{\partial\eta^2} = a\sigma\sin\phi\mathrm{e}^{-\sigma\eta}\frac{2}{\pi}\int_0^\infty \bar{\Omega}_t^0(\beta)\mathrm{e}^{-\epsilon\beta^2 T}\frac{1-\cos\beta\eta}{\beta^2}\,\mathrm{d}\beta. \tag{67}$$

A particular solution is

$$\tilde{w}_1^p = -a\sigma\sin\phi\mathrm{e}^{-\sigma\eta}\frac{2}{\epsilon\pi}\int_0^\infty \bar{\Omega}_t^0(\beta)\mathrm{e}^{-\epsilon\beta^2 T} \times\left(\frac{2\sin\beta\eta}{\sigma\beta(\sigma^2+4\beta^2)} + \frac{1-\cos\beta\eta}{\beta^2(\sigma^2+\beta^2)} + \frac{3\cos\beta\eta}{(\sigma^2+\beta^2)(\sigma^2+4\beta^2)}\right)\mathrm{d}\beta. \tag{68}$$

The homogeneous solutions that must be superimposed on the particular solution in order to satisfy the boundary condition at the wall as well as the initial condition are

$$\tilde{w}_1^{H_1} = a\sigma\sin\phi\frac{2}{\epsilon\pi}\int_0^\infty H(\beta)\mathrm{e}^{-\epsilon\beta^2 T}\cos\beta\eta\,\mathrm{d}\beta \tag{69}$$

and

$$\tilde{w}_1^{H_2} = a\sigma\sin\phi\frac{2}{\epsilon\pi}\int_0^\infty I(\beta)\mathrm{e}^{-\epsilon\beta^2 T}\sin\beta\eta\,\mathrm{d}\beta \tag{70}$$

with

$$H(\beta) = \frac{3\bar{\Omega}_t^0(\beta)}{(\sigma^2+\beta^2)(\sigma^2+4\beta^2)}.$$

Setting $\tilde{w} = 0$ at $T = 0$ determines that $I(\beta)$ is the Fourier sine transform of $-(\tilde{w}_1^{H_1}+\tilde{w}_1^p)$. The above represents an exact solution, and in theory the quadratures can be completed once the initial vorticity is specified. If the initial vorticity specification is in terms of known functions whose Fourier cosine transforms are relatively simple, then the quadratures might be done with the aid of extensive tables. However, it is certainly sufficient to specify the initial vorticity and then to resort to numerical quadrature to determine the solution.

Now the solution produced by specifying the normal vorticity at $T = 0$ is examined. As previously mentioned, this requires only the solution to the partial differential equation corresponding to the Squire mode. Since in wave space the normal vorticity

is proportional to the tangential velocities, the initial specification must be zero at the wall and is therefore written in terms of the Fourier sine transform or

$$\Omega_n(\tilde{\gamma},\eta,\phi) = \mathrm{i}\tilde{\gamma}\frac{2}{\pi}\int_1^\infty \bar{\Omega}_n^1(\beta)\sin\beta\eta\,\mathrm{d}\beta + o(1). \tag{71}$$

The solution is just

$$\tilde{w}_0 = \frac{2}{\pi}\int_0^\infty \bar{\Omega}_n^1(\beta)\mathrm{e}^{-\epsilon\beta^2 T}\sin\beta\eta\,\mathrm{d}\beta. \tag{72}$$

Here we see that an order-$\tilde{\gamma}$ initial normal vorticity produces an $O(1)$ velocity.

By examining the perturbation energy dependence on the normal vorticity, $\tilde{w} = \tilde{w}_0 + \tilde{\gamma}\tilde{w}_1$, it is evident why the algebraic growth is sensitive to the inclusion of non-zero initial normal vorticity. When considering initial vorticities scaled as above, the leading-order expression for G is

$$G \sim \frac{\displaystyle\int_0^\infty (\bar{\Omega}_n^1(\beta))^2\mathrm{e}^{-2\epsilon\beta^2 T}\,\mathrm{d}\beta + O(\tilde{\gamma}^2)}{\displaystyle\int_0^\infty (\bar{\Omega}_n^1(\beta))^2\,\mathrm{d}\beta + O(\tilde{\gamma}^2)}. \tag{73}$$

However, when $\Omega_n(\tilde{\gamma},\eta,\phi) = 0$ and therefore $\tilde{w}^0 = 0$, the leading-order expression for G is

$$G \sim \frac{\displaystyle\int_0^\infty \left(\frac{1+\beta}{\beta^2}\bar{\Omega}_t^0(\beta)\right)^2 \mathrm{e}^{-2\epsilon\beta^2 T}\,\mathrm{d}\beta + \frac{\pi^2}{4}\int_0^\infty |\tilde{w}_1|\,\mathrm{d}\eta}{\displaystyle\int_0^\infty \left(\frac{1+\beta}{\beta^2}\bar{\Omega}_t^0(\beta)\right)^2 \mathrm{d}\beta}. \tag{74}$$

In the first instance, G shows only decay to leading order. In the latter instance, the growth of $\tilde{w}_1$ is included in the leading order and thus there is algebraic instability. Therefore, it is seen that the case of zero initial normal vorticity is a singular case in the limit $\tilde{\gamma} \to 0$.

Since an analytic solution has been developed, it is necessary to compare against the numerically produced solution in the appropriate limit. Figure 7(*a*) shows the solution for $\tilde{w}_1$ for the parameter values $\tilde{\gamma} = 0.01$, $\epsilon = 0.002$, $\phi = 90^\circ$ to $T = 8000$ and $F(\eta) = \eta^2\mathrm{e}^{-\eta^2}$. It is seen that all qualitative features of the solution are properly captured by the leading-order solution (69) shown as the solid lines. Quantitatively, the leading-order solution loses accuracy as T increases which must be the case. Figure 7(*b*) and figure 7(*c*) show the solution to the same initial condition for values to $\tilde{\gamma} = 0.5$, for $T = 10$ and $T = 100$. Even for this relatively large value of $\tilde{\gamma}$, the small-$\tilde{\gamma}$ solution is still apparently valid.

7. Direct numerical simulation

In the previous sections, the temporal evolution of disturbances for the boundary layer flow have been presented. However, the boundary layer flow is truly investigated only in terms of a spatially-evolving flow. Unless a connection between the temporal and the spatial evolutions can be established, it will always be necessary to use the more difficult and expensive spatial calculations rather than the efficient temporal calculations. That there is such a connection for an unstable Tollmien–Schlichting wave is well known and is referred to as the Gaster transformation. No such relation has ever been shown for the transient period of the boundary layer. However, we have

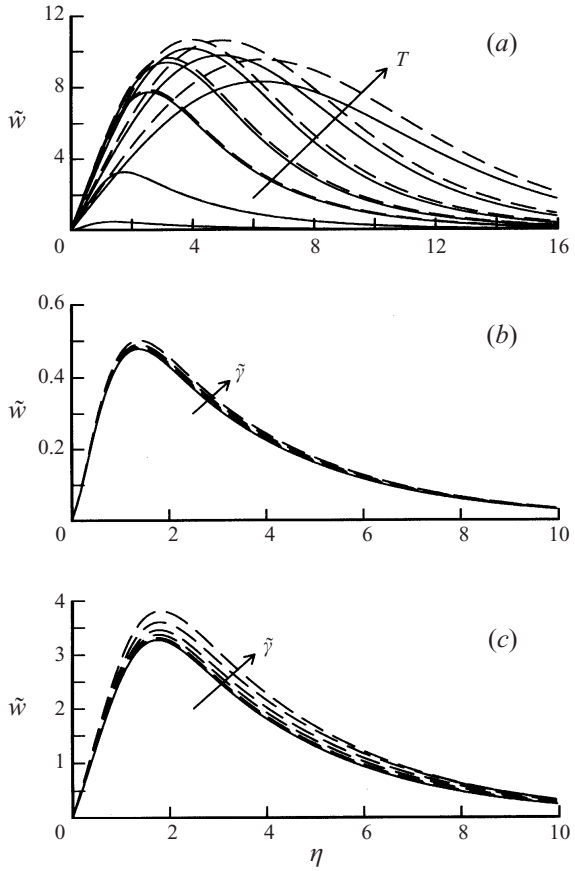

FIGURE 7. Comparison of analytical solution in the limit $\tilde{\gamma} \to 0$ (solid lines) and numerical solution (dashed lines). (*a*) $\tilde{\gamma} = 0.01$ and $T = 10$, 100, 500, 1000, 2000, 4000 and 8000. (*b*) $T = 10$ and $\tilde{\gamma} = 0.01$, 0.02, 0.05, 0.1, 0.2 and 0.5 (*c*) Same as (*b*) with $T = 100$.

previously discovered evidence of such a connection during the transient period for channel flow (Criminale *et al.* 1997). In what follows, evidence for such a connection in boundary layer flow is presented.

The numerical techniques required for the simulation and the disturbance forcing are briefly discussed below. For a detailed description of the spatial direct numerical simulation of the Navier–Stokes equations (DNS) approach used for this study, refer to Joslin, Streett & Chang (1992, 1993). The instantaneous velocities $\tilde{\boldsymbol{u}} = (\tilde{u}, \tilde{v}, \tilde{w})$ and the pressure $\tilde{p}$ are decomposed into steady base and disturbance components. The base flow is given by velocities $\boldsymbol{U} = (U, V, W)$ and the pressure P; the disturbance is given by velocities $\boldsymbol{u} = (u, v, w)$ and the pressure p. The velocities correspond to the coordinate system $\boldsymbol{x} = (x, y, z)$, where x is the streamwise direction, y is the wall-normal direction, and z is the spanwise direction. The base flow for the flat plate can be reasonably approximated by the Blasius similarity solution and the disturbance flow is found by solving the three-dimensional, incompressible Navier–Stokes equations. These equations are the momentum equation

$$\frac{\partial \boldsymbol{u}}{\partial t} + (\boldsymbol{u} \cdot \nabla)\boldsymbol{u} + (\boldsymbol{U} \cdot \nabla)\boldsymbol{u} + (\boldsymbol{u} \cdot \nabla)\boldsymbol{U} = -\nabla p + \frac{1}{Re}\nabla^2 \boldsymbol{u}, \tag{75}$$

and the continuity equation

$$\nabla \cdot \boldsymbol{u} = 0. \tag{76}$$

The boundary conditions in the far field are

$$\boldsymbol{u} \to 0 \quad \text{as} \quad y \to \infty \tag{77}$$

and the conditions at the wall are

$$\boldsymbol{u} = 0 \quad \text{at} \quad y = 0. \tag{78}$$

For parallel calculations, U is assumed to be a function of y only, and for non-parallel calculations U and V are functions of both x and y.

To solve equations (75) and (76) computationally, the spatial discretization entails a Chebyshev collocation grid in the wall-normal direction, fourth-order finite differences for the pressure equation, sixth-order compact differences for the momentum equations in the streamwise direction, and a Fourier sine and cosine series in the spanwise direction on a staggered grid (Joslin *et al.* 1993). For time marching, a time-splitting procedure is used with implicit Crank–Nicolson differencing for normal diffusion terms and an explicit three-stage Runge–Kutta method (Williamson 1980). The influence-matrix technique is employed to solve the resulting pressure equation (Helmholtz–Neumann problem) (Streett & Hussaini 1991; Danabasoglu, Biringen & Streett 1991). At the inflow boundary, the perturbation used corresponds to that used in the theory with an imposed initial amplitude of 10^{-7} such that the transient disturbance remains small so that comparisons to linear theory can be made. At the outflow, the buffer-domain technique of Streett & Macaraeg (1989) is used. The numerical code was run for sufficient time such that steady state has been achieved in a region which includes all of the relevant spatial growth.

The simulations used a grid of 1981 streamwise, 61 wall-normal, and 5 spanwise grid points (spanwise symmetric). The far-field boundary is located 50 displacement thicknesses from the wall, the streamwise distance is 1925 displacement thicknesses from the inflow, and the spanwise distance is $2\pi/\beta$. Both the wavenumber β and the Reynolds number were varied for the test cases listed in table 2. For the time marching, a time-step size of 0.5 is chosen for the three-stage Runge–Kutta method. Each computation required approximately 20 Cray Y/MP hours using a single processor to converge to a time-invariant solution. The choice of grid, computational domain size, and time-step size were based on previous experience described in Joslin *et al.* (1992, 1993). A grid refinement was performed by decreasing the domain size (as opposed to conventional increasing the number of grid points) to verify that grid-independent solutions were obtained.

Figures 8(*a*), 8(*b*) and 8(*c*) show the normalized energy density E_s as a function of streamwise distance x, calculated at steady state for $\tilde{\gamma} = 0.65$ and three values of the Reynolds number Re. The initial condition is chosen to be the first mode of subspace 2 given in (34). As suggested from temporal theory, there is significant transient growth and subsequent decay. Also shown in this figure as a dashed curve is the normalized energy E_T from the temporal solutions scaled in such a way that both the amplitude and location of the maxima coincide. To properly match with the E_s from the DNS calculations, E_T is defined as follows:

$$E_T = \int_0^\infty \left[|(\breve{u} - \breve{u}_\infty)^2| + |(\breve{v} - \breve{v}_\infty)^2| + \lambda^2 |(\breve{w} - \breve{w}_\infty)^2| \right] \mathrm{d}y, \tag{79}$$

Case	Subspace	Re	β	a_i	b_i
1	2	500	0.65	0.766	0.634
2	2	1000	0.65	0.768	0.636
3	2	1500	0.65	0.770	0.636
4	2	500	0.80	0.624	0.714
5	2	1500	0.80	0.626	0.715
6	2	500	0.95	0.544	0.774
7	2	500	1.20	0.473	0.857
8	2	500	1.40	0.443	0.916
9	2	500	2.00	0.401	1.079

TABLE 2. Test cases for theoretical validation with DNS.

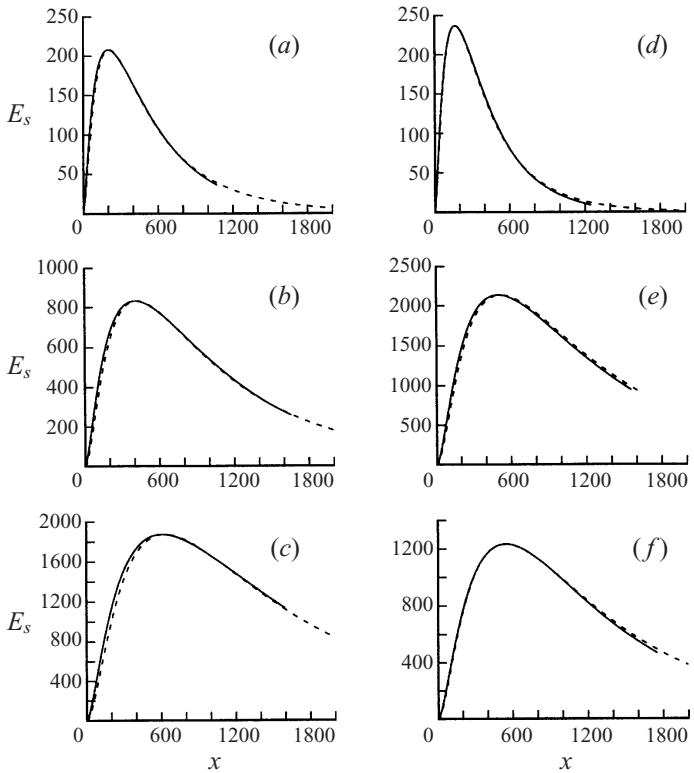

FIGURE 8. Normalized energy density E_s vs. streamwise distance. Spatial calculations (solid) compared with scaled temporal calculations (dashed). Initial condition is first mode of subspace 2 and $\phi = 90°$. (*a*) $R = 500$ and $\tilde{\gamma} = 0.65$, (*b*) $R = 1000$ and $\tilde{\gamma} = 0.65$, (*c*) $R = 1500$ and $\tilde{\gamma} = 0.65$, (*d*) $R = 500$ and $\tilde{\gamma} = 0.8$, (*e*) $R = 1500$ and $\tilde{\gamma} = 0.8$, and (*f*) $R = 1000$ and $\tilde{\gamma} = 0.65$ using subspace 3.

where

$$\lambda = \delta^{*2}\tilde{\gamma}^2/(2\pi),$$

scaled in such a way that $E_T = 1$ at $t = 0$. The temporal results are obtained by solving equations (12) and (13) subject to the same initial conditions. The temporal results were scaled as follows:

$$x = a_i t, \qquad E_T = b_i E(t), \tag{80}$$

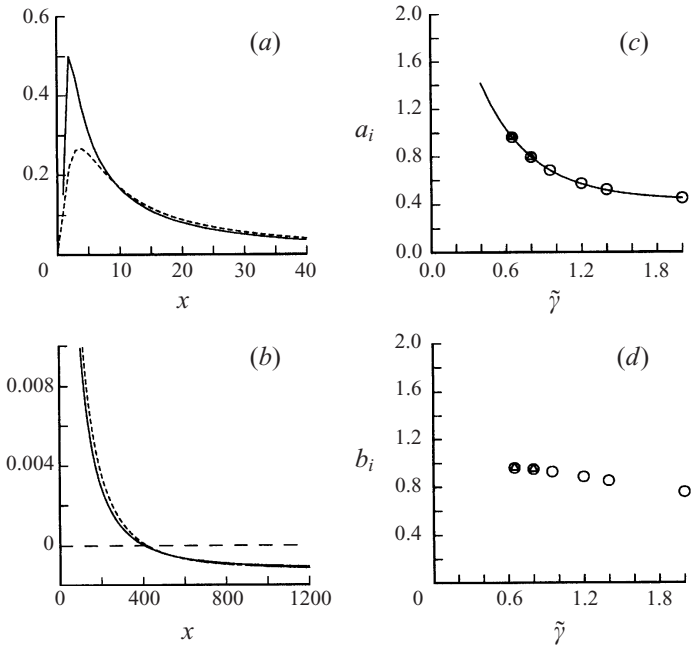

FIGURE 9. Comparison of spatial and temporal growth rates for $Re = 10^3$. (*a*) Transformation does not hold for small x. (*b*) Transformation does hold over the region where transient growth is a maximum. (*c*) Values of a_i, solid line is empirical fit given by (83), circles, $Re = 500$. (*d*) Values of b_i.

where the scaling constants a_i and b_i are given in table 2 for each case listed. As can be seen, there is considerable agreement between the two, hinting at the possibility of a spatial–temporal transformation. Further insight into this possibility is explored in figures 9(*a*) and 9(*b*) where the growth rates as a function of x are shown. The growth rates for both the spatial and temporal solutions are defined in the following manner:

$$\frac{1}{E_s}\frac{\mathrm{d}E_s}{\mathrm{d}x} = \alpha(x), \qquad \frac{1}{E(t)}\frac{\mathrm{d}E(t)}{\mathrm{d}t} = \omega(t). \tag{81}$$

By using the previous relationship between x and t, the growth rates are identically zero at the same value of x. A relationship of the form

$$\alpha(x) = \frac{\omega(x/a_i)}{c}, \qquad c = 1, \tag{82}$$

holds over most of the domain except for the very early transients. This value of c corresponds to the non-dimensional mean velocity at infinity. To show that the relationship between ω and α hold throughout other regions in the (α, Re)-plane, figures 8(*d*) and 8(*e*) show results for $\tilde{\gamma} = 0.8$. It is interesting to note that a similar result is found for the channel flow problem but with $c = 1/2$ (Criminale *et al.* 1997). Thus, there is strong evidence of a correspondence between spatial and temporal calculations for the transients as well as the previously known connection for the long-time asymptotic solutions given by the Gaster transformation. If a spatial-temporal relationship could be determined, then the efficient temporal theory could be used to study the spatial problem at a fraction of the cost of a DNS study.

In figures 9(*c*) and 9(*d*), the coefficients a_i and b_i as functions of β are shown. The

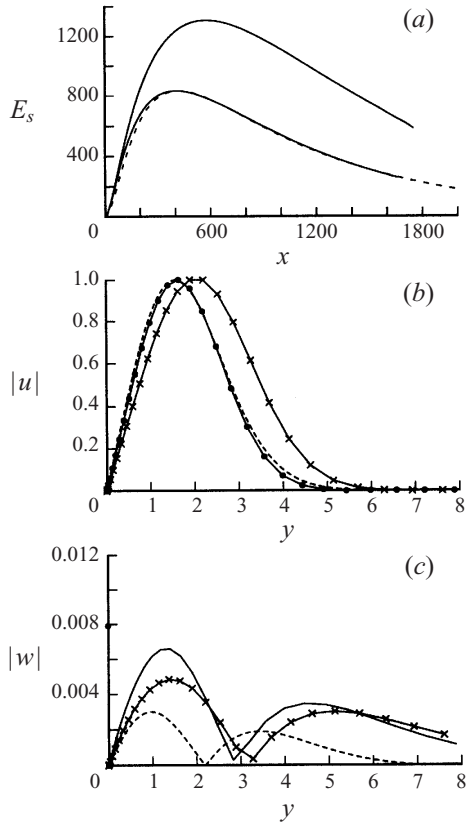

FIGURE 10. (*a*) Comparison of parallel and non-parallel spatial calculations with first mode of subspace 2 as initial condition. (*b*) Streamwise disturbance profiles at the x location where parallel calculations have their maxima: parallel temporal (dashed), parallel spatial (solid with circles) and non-parallel spatial (solid with crosses). (*c*) Spanwise disturbance profiles.

cases for $Re = 500$ are shown as open circles, while the other cases are shown as triangles. Surprisingly, all the data fall on an exponential curve, shown as the solid curve. The curve is given by

$$\frac{x}{t} = A\mathrm{e}^{-B\beta} + C, \tag{83}$$

where

$$A = -1.1401, \qquad B = 0.7360, \qquad C = 1.3406.$$

Therefore, at least for this particular case, a spatial–temporal relationship can be established.

The above connection applies to other inflow conditions. Figure 8(*f*) shows the results of a calculation using inflow conditions from subspace 3 of (35) with $R = 10^3$. This case is different from the previous one in that the inflow disturbances do not vanish in the free stream. Again, there is excellent agreement between the spatial and temporal calculations. The results of a non-parallel spatial calculation using inflow conditions from subspace 2 of (34) are shown in figure 10(*a*). For comparison, the results of the parallel calculations previously plotted in figure 8(*b*) are shown. Note that the effect of non-parallelism increases the maximum transient growth by over 50%. Thus the concept of algebraic instability, previously explored only for parallel

flows, is also seen to exist in real flows where the non-parallel nature cannot be ignored. The reason for the larger growth is shown in figures 10(*b*) and 10(*c*) where the velocity profiles are compared at the x-location where the parallel calculations have their maxima. The results from the temporal (dashed curve) and the spatial (solid curve with circles) calculations show excellent agreement in the streamwise disturbance velocity and qualitative agreement for the spanwise disturbance velocity which is several orders of magnitude smaller than the streamwise velocity component. Also shown in this figure are the results from the non-parallel spatial calculations, shown as a solid curve with crosses. The additional disturbance energy is seen to result from a broader profile which might be expected since the boundary layer thickness grows downstream.

8. Conclusions

The Blasius boundary layer in an incompressible viscous fluid subject to the influence of small perturbations has been investigated. Instead of using the techniques of classical stability analysis or the more recent techniques involving eigenfunction expansions, the approach has been to first Fourier transform the governing disturbance equations in the streamwise and spanwise directions only and then solve the resulting partial differential equations numerically by the method of lines. Unlike traditional methods where travelling wave normal modes are assumed for solution, this approach offers an alternative means whereby arbitrary initial input can be specified. Thus, arbitrary initial conditions can be imposed and the full temporal behaviour, including both early-time transients and the long-time asymptotics, can be determined. All of the stability data that are known for such flows can be reproduced. The details of the early-time transients are explored by considering a series of initial value problems. The first set of initial value problems is designed to determine the effect of disturbance location. For unstable conditions, a localized initial velocity disturbance always excites the unstable Tollmien–Schlicting wave, even when the disturbance lies far outside the boundary layer. For stable conditions, the degree of transient growth is found to depend on the location of the localized disturbance, with localized disturbances within the boundary layer showing greater transient growth. For fixed disturbances, the transient growth is seen to depend greatly on the wavenumber. The next set of initial value problems is designed to determine both the maximum possible transient growth and the likelihood that such a transient growth would occur for arbitrary disturbances. For this purpose, an optimization scheme is presented using three discrete sets of orthogonal functions, each set with a different characteristic behaviour in the free stream. Using these orthogonal sets, it is determined what type of initial conditions are necessary to produce almost the same maximum growth that the governing equations allow. Although these sets are discrete, they are only used to specify the initial conditions and not to solve the equations; therefore, the contribution of the continuum to the conditions producing the maximum transient growth is properly included. Disturbances that are non-zero and non-localized in the free stream produce the greatest transient growth. However, large transient growth is to be found only in response to disturbances with zero initial normal vorticity. When non-zero normal vorticity is included in the initial conditions, the transient growth is either greatly diminished or eliminated. An analytic theory is presented that resolves the role of the initial normal vorticity in determining the subsequent transient growth. Furthermore, the analysis results in a relatively simple solution that properly accounts for the entire spectrum of eigenfunctions and an explicit solution

of the Squire equation is found. Finally, direct numerical simulation of the spatial problem is carried out and compared to the linear temporal theory. It is conclusively shown that there exists a connection between spatial and temporal calculations even during the transient period. The theoretical connection suggests that the important problems of receptivity and control can be explored using a temporal theory, and it would be expected that the results would then apply to the spatial theory.

The authors would like to thank their good friend C. E. Grosch of Old Dominion University for all of his help, insights and encouragement. This work was supported by the National Aeronautics and Space Administration under NASA Contract No. NAS1-19480 while in residence at the Institute for Computer Applications in Science and Engineering (ICASE), NASA Langley Research, Hampton, VA 23681-0001, USA.

REFERENCES

Ames, W. F. 1977 *Numerical Methods for Partial Differential Equations.* Academic.

Benney, D. J. & Gustavsson, L. H. 1981 A new mechanism for linear and nonlinear hydrodynamic instability. *Stud. Appl. Maths* **64**, 185–209.

Breuer, K. S. & Haritonidis, J. H. 1990 The evolution of a localized disturbance in a laminar boundary layer. Part 1. Weak disturbances *J. Fluid Mech.* **220**, 569–594.

Breuer, K. S. & Kuraishi, T. 1994 Transient growth in two- and three-dimensional boundary layers. *Phys. Fluids* A **6**, 1983–1993.

Breuer, K. S. & Landahl, M. T. 1990 The evolution of a localized disturbance in a laminar boundary layer. Part 2. Strong disturbances. *J. Fluid Mech.* **220**, 595–691.

Butler, K. M. & Farrell, B. F. 1992 Three-dimensional optimal perturbations in viscous shear flow. *Phys. Fluids* A **4**, 1637–1650.

Criminale, W. O. & Drazin, P. G. 1990 The evolution of linearized perturbations of parallel flows. *Stud. Appl. Maths* **83**, 123–157.

Criminale, W. O. & Drazin, P. G. 1998 Initial-value problems of parallel flows of a fluid of small viscosity. *Phys. Fluids* (submitted).

Criminale, W. O. & Kovasznay, L. S. G. 1962 The growth of localized disturbances in a laminar boundary layer. *J. Fluid Mech.* **14**, 59–80.

Criminale, W. O., Jackson, T. L., Lasseigne, D. G. & Joslin, R. D. 1997 Perturbation dynamics in viscous channel flows. *J. Fluid Mech.* **339**, 55–75.

Danabasoglu, G., Biringen, S. & Streett, C. L. 1991 Spatial simulation of instability control by periodic suction and blowing. *Phys. Fluids* **3**, 2138.

Goldstein, M. E. & Hultgren, L. S. 1989 Boundary layer receptivity to long wave free-stream disturbances. *Ann. Rev. Fluid Mech.* **21**, 137–166.

Grosch, C. E. & Salwen, H. 1978 The continuous spectrum of the Orr–Sommerfeld equation. Part 1. The spectrum and the eigenfunctions. *J. Fluid Mech.* **87**, 33–54.

Gustavsson, L. H. 1979 Initial-value problem for boundary layer flows. *Phys. Fluids* **22**, 1602–1605.

Gustavsson, L. H. 1991 Energy growth of three-dimensional disturbances in plane Poiseuille flow. *J. Fluid Mech.* **224**, 241–260.

Gustavsson, L. H. & Hultgren, L. S. 1980 A resonance mechanism in plane Couette flow. *J. Fluid Mech.* **98**, 149–159.

Hill, D. C. 1995 Adjoint systems and their role in the receptivity problem for boundary layers. *J. Fluid Mech.* **292**, 183–204.

Hultgren, L. S. & Gustavsson, L. H. 1980 Algebraic growth of disturbances in a laminar boundary layer. *Phys. Fluids* **24**, 1000–1004.

Joslin, R. D., Streett, C. L. & Chang, C.-L. 1992 Validation of three-dimensional incompressible spatial direct numerical simulation code. – A comparison with linear stability and parabolic stability equations theories for boundary-layer transition on a flat plate. *NASA TP*-3205.

Joslin, R. D., Streett, C. L. & Chang, C.-L. 1993 Spatial direct numerical simulation of boundary-layer transition mechanisms: validation of PSE theory. *Theor. Comput. Fluid Dyn.* **4**, 271.

KELVIN, LORD 1887 Stability of fluid motion – Rectilinear motion of viscous fluid between two parallel plates. *Phil. Mag.* **24**, 188–196.

LIGHTHILL, M. 1963 Introduction to boundary layer theory. In *Laminar Boundary Layer* (ed. L. Rosenhead). Oxford.

MACK, L. M. 1976 A numerical study of the temporal eigenvalue spectrum of the Blasius boundary layer. *J. Fluid Mech.* **73**, 497–520.

ORR, W. M'F. 1907*a* The stability or instability of the steady motions of a perfect liquid and a viscous liquid. Part I. *Proc. R. Irish. Acad.* **27**, 9–68.

ORR, W. M'F. 1907*b* The stability or instability of the steady motions of a perfect liquid and a viscous liquid. Part II. *Proc. R. Irish. Acad.*, **27**, 69–138.

REDDY, S. C. & HENNINGSON, D. S. 1993 Energy growth in viscous channel flows. *J. Fluid Mech.* **252**, 209–238.

SALWEN, H. & GROSCH, C. E. 1981 The continuous spectrum of the Orr–Sommerfeld equation. Part 2. Eigenfunction expansions. *J. Fluid Mech.* **104**, 445–465.

SOMMERFELD, A. 1949 *Partial Differential Equations in Physics*. Lectures in Theoretical Physics, Vol. 6, Academic Press.

STREETT, C. L. & HUSSAINI, M. Y. 1991 A numerical simulation of the appearance of chaos in finite-length Taylor-Couette flow. *Appl. Numer. Maths* **7**, 41–71.

STREETT, C. L. & MACARAEG, M. G. 1989 Spectral multi-domain for large-scale fluid dynamic simulations. *Intl J. Appl. Numer. Maths* **6**, 123.

TREFETHEN, L. N., TREFETHEN, A. E., REDDY, S. C. & DRISCOLL, T. A. 1993 Hydrodynamic stability without eigenvalues. *Science* **261**, 578.

WILLIAMSON, J. H. 1980 Low-storage Runge-Kutta schemes. *J. Comput. Phys.* **35**, 48.